THESIS

SNOWFALL-DRIVEN TOPOGRAPHIC EVOLUTION:

IMPACTS ON SNOW DISTRIBUTION PATTERNS

Submitted by

Alexander Richard Olsen-Mikitowicz

Department of Ecosystem Science and Sustainability

In partial fulfillment of the requirements

For the Degree of Master of Science

Colorado State University

Fort Collins, Colorado

Fall 2023

Master's Committee:

Advisor: Steven Fassnacht

Daniel McGrath
Stephen Leisz

ABSTRACT

SNOWFALL-DRIVEN TOPOGRAPHIC EVOLUTION:

IMPACTS ON SNOW DISTRIBUTION PATTERNS

This study develops a scalable meteorologically independent snow accumulation model to better estimate snowpack depth using an enhanced representation of actual processes. Current snow accumulation models incorporate bare or snow-free surface properties derived from elevation, aspect, vegetation, and prevailing wind characteristics to determine the drivers of snow distribution yet neglect to consider how subsequent snowfalls can reshape the initial terrain conditions. We hypothesize that a snow depth model that accumulates snowfall while accounting for the antecedent snow-affected surface characteristics is more representative of natural processes and will therefore yield more accurate depth estimates than models that reference a snow-free topographic surface. To address this premise, the research explores (1) conducting a sensitivity analysis to evaluate the behavior of both models, (2) determining the differences between the two snow accumulation modeling approaches, and (3) assessing each model's performance in different location, scale, and temporal resolution conditions to determine their resiliency and transferability.

Terrestrial LiDAR was employed at two field sites following snow deposition events and captured a range of spatial extents and resolutions. The Upper Piceance Creek (UPC) site near Meeker, CO covered approximately 10 m^2 at centimeter resolution; the Izas Experimental Catchment in the Spanish Pyrenees covered 1 km^2 at meter resolution. A regression tree machine learning model was utilized to estimate snow depth based on 14 topographic features. This process engaged in two mechanisms: 1. Static method, where snow depth (ds_t) determined from the bare earth digital terrain model (ds_0) was estimated with snow-free topographic features and 2. Dynamic method, where snow

depth (ds_t) determined from the previous snow surface height (ds_{t-1}) was estimated with the ds_{t-1} snowfall affected surface. The analyses found that the models were resilient to changes in training allocations under a random sampling method, but sensitive to both the prevailing wind direction used for feature creation and the overall resolution used to represent surface features. The primary difference between the static and dynamic models for snow depth estimates was the number of features used and their relative importance. The static method had a higher overall median importance and relied mainly on Directional Relief and Relative Topographic Position for snow depth estimates, while the dynamic method displayed lower overall median importance but utilized more surface features over a single accumulation season. The dynamic method outperformed the static method at UPC by approximately 0.07 in a Nash-Sutcliffe efficiency comparison, and only 0.01 at Izas Experimental Catchment suggesting issues with process-scale representation of snow accumulation at the Izas site.

ACKNOWLEDGEMENTS

First and foremost, I would like to thank my advisor Steven Fassnacht, Ph.D. for his time and mentorship throughout this journey. Steven and I first met in an arrival gate at Frankfurt International Airport in December 2016 at the outset of a brief study abroad program exploring the Douro River in Spain and Portugal. At the time, I had no idea what a significant impact being in his sphere of influence would have on my life and career. After graduating with my bachelor's degree and lacking some direction, he graciously offered me the opportunity to work in his graduate lab focusing on snow in whatever capacity I found intriguing. With the beginning of my research complicated by a global pandemic and a brief hiatus while I traveled around the country flying UAV's, Steven always supported me and withheld any frustrations with my extended enrollment. Steven is a brilliant professor who takes great pride in teaching others how to think scientifically so they may find their place in this world and possess the tools to improve it. I am truly honored to call him both mentor and friend.

This research was in part made possible through funding from the Colorado Water Center and National Institutes for Water Resources 2020 grant. Thank you to the many others who have helped me along the way. Many thanks to the committee members for their time, input, and expertise throughout this process. To Jessica Sanow, Ph.D. for her meticulous snow mapping efforts and generosity with these data which serve as the backbone of this analysis and Jesús Revuelto, Ph.D. and others for collecting and sharing the Izas dataset with aspiring snow scientists all over the world. Finally, to all my family, friends, and fellow graduate student lab mates for their continued encouragement and support over the years. It really takes a village.

DEDICATION

The work and knowledge herein are dedicated to my wonderful parents Marlene and Walter who have loved and supported me through all my endeavors, accomplishments, and especially my failures. I owe my introduction and fascination with snow to them which was forged over many memorable ski trips to Purgatory resort near Durango where it's important to remember:

The love-boat sushi platter is a bad deal! . . .

TABLE OF CONTENTS

1. INTRODUCTION

1.1 Snow as a Natural Resource

In Frank Herbert's science fiction epic, "Dune" (Herbert, 1965), the declaration of the desert dwelling Fremen, "This is the bond of water. A man's flesh is his own; the water belongs to the tribe," serves as an unadorned reminder that fresh water is not only the lifeblood of our societies but the very foundation of our existence. While Earth may not face the same extreme scarcity of fresh water as the setting in the novel, it remains a finite and essential resource that requires careful management to support a growing global population. The hydrosphere encompasses the entirety of Earth's water, and according to estimates by the U.S. Geological Survey, merely 3% of this reservoir is composed of fresh water. However, only 1/6th of that fresh water readily accessible, where the rest remains locked in polar ice caps, buried deep underground, or suspended in the atmosphere. The primary sources of this available fresh water include groundwater, surface water runoff, and snow (U.S. Geological Survey, 2022)

As a critical source of fresh water, snow serves many important roles within the hydrologic cycle. In addition to being a source of fresh water, snow also acts as a water storage system or a natural reservoir giving supply to many rivers. A significant portion of the water flow in the Colorado River and various other Southwestern U.S. rivers stems from the annual thaw of mountain snowpack (Serreze et al., 1999). In addition to supplying much of the water itself to these river systems, snow also provides an important timing and attenuation control on the water it slowly releases and the shape, peak, and duration of the snowmelt hydrograph are often controlled by the spatial pattern of the snowpack (Luce et al., 1998; Pomeroy et al., 2009). The presence of snow on the landscape also influences surface properties, including albedo, the surface radiation budget, and turbulent surface-atmosphere fluxes (Peixóto and Oort, 1992). Beyond these immediate effects, snow plays a pivotal role in shaping the global climate and energy exchange, making it a crucial component of the Earth's natural systems.

As a source of fresh water in many parts of the world, snow supports the vitality of ecosystems and the prosperity of human societies. In the Colorado River Basin, the rivers fueled by snowmelt play a fundamental role in satisfying the water demands of approximately 38 million individuals and sustaining nearly 4–6 million acres of irrigated agriculture (United States Bureau of Reclamation, 2012; Cohen et al., 2013). In addition to providing water for urban centers, snowmelt driven rivers achieve additional purposes, including replenishment of storage reservoirs like the at-risk Lake Powell (Myers, 2013), recharge of groundwater aquifers (Carroll et al., 2019), and the mechanism behind hydropower generation systems (Schaefli et al., 2007). Snow also exerts a substantial economic influence in numerous regions that extend beyond its evolution into water. Winter sports are enjoyed by millions and have become significant business sectors within state and local economies. In 2016, the economic impact of skiing and snowmobiling in Colorado amounted to $2.56 billion, supported over 43,000 jobs in related industries (Hagenstad et al., 2018), and the annual global economic impact of snow is estimated to be in the trillions (Sturm, 2017). Snow also plays a key ecological role as a critical habitat, providing a vital shelter for various species. Throughout the winter, many animals rely on the subnivean zone for its thermal resistance and structural stability, which support essential processes such as reproduction, thermoregulation, and predation avoidance (Glass et al., 2021).

1.2 Snow Measurement Methodology

Snow measurements are important for water resource planning, especially in water limited regions like western United States dominated by mountain snowpack where 60-75% of annual streamflow originates from snowmelt (Doesken and Judson, 1996). The connection between winter snowpack metrics and available runoff in the spring and summer was established in the early 1900's via manual snow course measurements (Church, 1908). Snow courses consist of a series of measurements that provide information about the quantity of water associated with a given snowpack or snow water equivalent (SWE), where SWE is calculated as the product of snow depth (d_s) and density (ρ_s). Snowpack monitoring in the western U.S. has since evolved to a more regionally distributed system, with the Natural Resources Conservation Service (NRCS) oversight of the Snow Telemetry Network (SNOTEL). The SNOTEL network consists of over 900 automated data collection sites strategically situated in remote mountainous watersheds (U.S. Department of Agriculture, Natural Resources Conservation Service). These stations gather and disseminate snowpack, precipitation, temperature, and other climatic data to the National Water and Climate Center where it is analyzed and used to inform runoff forecasting and water management decision making.

Recent decades in snow mapping and measurement have been characterized by a shift away from both manual and automated point-based measurements to the adoption of sophisticated remote sensing techniques, ushering in a new era of snowpack assessment. Point-based snow measurements from sources like SNOTEL alone can be a poor indicator of snow over large areas and complex environments like mountainous terrain (Molotch and Bales, 2005; Guan et al., 2013, Meromy et al., 2013). Light Detection and Ranging (LiDAR) systems are tools with the ability to capture precision target positions and snow surfaces with high spatial resolution in rough terrain and forested regions (Lefsky et al., 2002; Hopkinson et al., 2004). These highly precise mapping systems geolocate by coupling ranging lasers with geographic positioning systems (GPS) for ground based terrestrial laser scanning (TLS) systems or with inertial measurement units when affixed to airborne platforms (Deems et al., 2013). TLS systems have been employed at the catchment-scale (Egli et al., 2012; Revuelto et al., 2014) and airborne systems for basin-scale (Painter et al., 2016) snow depth mapping with excellent results. After acquiring LiDAR data from both the ground surface and snow-affected terrain, the subtraction of co-registered point clouds yields snow depth maps with high spatial resolution (Deems et al., 2013). While manual point-based snow mapping techniques have traditionally been labor-intensive and area limited, the transition to remotely sensed measurements is an advancement in efficiency, coverage, and resolution. However, it is important to recognize both approaches hold distinct value to accurate snow mapping.

1.3 Snow Measurement Challenges

The foremost challenge in quantifying snow in mountainous regions lies in achieving accurate and precise representations of snow distributions given the myriad of forces acting upon it. It has been widely established that snow depth and density vary both spatially and temporally (Borman et al., 2013; López-Moreno et al., 2013; Fassnacht et al., 2018) especially in mountain and alpine terrain (Buisan et al., 2015) with these heterogeneities resulting from processes occurring at different scales (Blöschl, 1999; Clark et al., 2011). Some of the major processes contributing to the variation in the spatial distribution of snow include incident shortwave radiation and the absorption and emission of most long-wave radiation (Male, 1980), snow crystal metamorphism and settling (Colbeck, 1982), redistribution by wind (Schmidt, 1982), and sublimation and interception by vegetation which can comprise 13-31% of annual snowfall depending on forest canopy type (Pomeroy et al., 1998).

In the operational context of snow hydrology, accurate snow depth data are critical to the determination of snow water equivalent. While the snow depth parameter makes up half of the SWE equation, it has been empirically established that the spatial variability of snow density is smaller than that of snow depth (López-Moreno et al., 2013). Sufficient SWE estimates can be made based on snow depth paired with assumptions of bulk snow density facilitated by modeling techniques and historical data (Jonas et al., 2009; Sturm et al., 2010, McCreight and Small, 2013). This emphasis on precise spatial snow depth distributions provides a foundational component for greater hydrologic assessments, making it a key consideration in the broader understanding of snowpack dynamics.

The ongoing challenge due to the spatiotemporal variation in snow has garnered increased attention within the realm of snow research. Expanding snow measurement efforts along with more thoroughly evaluated sampling strategies for collecting ground-truth measurements to improve snow estimation techniques have been called for from within the discipline (Fassnacht, 2021). As remotely sensed snow products become assimilated into larger data structures, it becomes increasingly essential to improve our understanding of the uncertainties surrounding the spatiotemporal distribution of snow, a crucial aspect in addressing the most significant problem in snow hydrology – accurate estimation of mountain SWE (Dozier et al., 2016).

1.4 Snow Distribution: Relationships & Uncertainty

Considerable research has been dedicated to a better understanding of the spatial distribution of snow and the associated variables impacting snow depth. Prior to the implementation of contemporary remote sensing techniques like LiDAR, point measurements were used with statistical methodologies to assess the factors influencing snow distributions. Early efforts to understand the controls on snow distributions showed that snow accumulation was related to elevation and forest canopy (Meiman et al., 1969). Furthering the idea, the use of statistical techniques like binary regression tree (BRT) models found that partitioning SWE sampling into zones based on topographic and radiation variables yielded superior estimates over random samples (Elder et al., 1991). Evaluations of the relative performance of different spatial interpolation methods for snow depth estimates suggested BRT models were superior to inverse distance weighting and kriging but independent variables including elevation, slope, aspect, net solar radiation, and vegetation were only sufficient at explaining 18-30% of the snow depth variability (Erxleben et al., 2002). A general additive model improved the estimates of the spatial distribution of snow depth explaining up to 73% of the variance using additional geographic and topographic variables and supporting non-linear relationships (Lopez-Moreno and Nogués-Bravo, 2005). More recently, the combination of high-resolution TLS acquisitions (1 m^2) and machine learning algorithms identified two highly important topographic snow depth predictors, topographic position index and maximum upwind slope, while explaining 82-94% of the snow depth variance in a catchment (Revuelto, et al., 2020).

In addition to spatial structure, snow distributions also exhibit a temporal dimension characterized by inter- and intra-seasonal patterns. Research into the temporal relationship of snow distribution has found strong interannual consistency of spatial patterns of snow depth from TLS and airborne LiDAR scans (Lopez-Moreno and Vicente-Serrano, 2007; Deems et al., 2008; Mendoza et al., 2020). Inter-seasonal snow depths may differ in absolute magnitude, but deep and shallow zones occur in the same location (Mason, 2020). Fractal analyses of snow depth discovered spatial consistencies at shorter ranges of 15-40 meters (Deems et al., 2008), longer-ranges of 185-300 meters in the direction of dominant winds (Mendoza et al., 2020) and that the variability of resolutions required to detect these consistencies suggests appropriate scaling of measurements is required for accurate representations of snowpack characteristics over time (Fassnacht and Deems, 2006). The inter-seasonal consistency of the spatial patterns observed in snow depth also extended to the topographic controls on the spatial distribution of snow depth (Erickson et al., 2005) where potential solar radiation and a measure of exposure or shelter to wind (Winstral et al., 2002) were statistically significant year to year. However, the spatial distribution of snow and the relationship to topographic influences from an intra-seasonal perspective is less well understood beyond the dynamic processes mentioned in section 1.3. From the intra-seasonal basis, topographic surface characteristics can undergo significant transformations caused by the addition, accumulation, and redistribution of snow whereas these features tend to stay the same from an inter-seasonal context.

1.5 Machine Learning and Applications

The integration of more powerful technologies and innovative methods, including the concept of machine learning within the field of artificial intelligence, stimulates new possibilities in the spatial analyses of snow. Advances in computer science have opened the accessibility of artificial intelligence methodologies, where they are commonly incorporated into research processes. These data-intensive machine learning methods are proliferating across diverse fields, facilitating evidence-based decision making in areas such as healthcare, manufacturing, education, financial modeling, policing, marketing, and more (Jordan and Mitchell, 2015). As the practice of machine learning rapidly expands, it will present many methodological opportunities which match very well with the needs and challenges of hydrological research (Lange and Sippel, 2020).

Machine learning is a subdivision of artificial intelligence defined by algorithms capable of learning from data that can make decisions based on observed patterns but require human intervention to correct a wrong decision or conclusion. Machine learning is further classified into supervised, unsupervised, and reinforcement learning based on the type of problem being addressed. Within the supervised learning category of approaches are applications concerning classification and regression, the latter of which is explored in this research. Fundamentally, machine learning algorithms construct a model using training data and then utilize test data to make informed decisions or generate predictions. Regression machine learning methods like random forests are excellent tools for geospatial applications due to their recognition of complex patterns and relationships, identification of relevant features, and efficiency with large data volumes (Döllner, 2020) and the integration with remotely sensed products presents a promising avenue to address and reduce uncertainties in the estimation of snow data (Oroza et al., 2016). Exploring Intra-seasonal variations in snow depth distributions and their associations with evolving topographic structures via machine learning tools offers a compelling framework for improving the accuracy of snow depth estimates in mountainous terrain.

1.6 Research Questions and Objectives

The purpose of this study is to introduce a novel approach in representing snow accumulation, thereby aiming to improve snow distribution modeling. As snow falls, redistributes, and settles, it reshapes the landscape, thus changing the initial conditions upon which subsequent snow accumulates. Current snow distribution and modeling approaches accumulate snow onto an initial surface or bare ground. Specifically, the terrain as represented with static conditions of elevation, slope, aspect, and topographic position are constant throughout the accumulation period. This current research seeks to improve the formulation of the snow accumulation process by asking the following questions: (1) does the change in the shape of the snow surface influence the nature of subsequent snow accumulation patterns, and (2) how does scale influence this snow accumulation. The hypothesis is that using variable snow-affected surfaces for accumulation over the winter season yields more accurate snow depth estimates than using a static bare ground surface. By considering natural processes, these variable surface accumulation models are expected to provide improved representations of snow depth. The hypothesis is addressed with the following objectives: (1) conduct a sensitivity analysis of the models to evaluate the behavior of the static and dynamic method, (2) determine the difference between static and dynamic machine learning snow accumulation modeling approaches, and (3) assess the model performance in different location, scale, and temporal resolution conditions to determine their reliability and applicability. To accomplish these objectives, we evaluated snow data collected at two geographically separate locations with distinct spatiotemporal resolutions.

2. SITE DESCRIPTION

2.1 Primary Site: Upper Piceance Creek

The Upper Piceance Creek (UPC) site serves as the focal point for this study. Situated approximately 35 km south of Meeker, Colorado, in the Rocky Mountain region of the western U.S., the site spans a small-scale area of 27 m^2 and sits at an elevation of 2,100 m above sea level (Figure 2-1). The UPC field site has a warm summer continental climate in the Köppen and Geiger Climate Classification (subtype Dfb). On-site sensors recorded hourly from November 2019 to March 2020 yielded an average temperature of -4.1°C (-7.9°C min, 1.6°C max) and average dewpoint temperature of -8.7°C (-12.3°C min, -3.5°C max). Grasses, sagebrush, juniper, and other species from the mountain shrub ecological community occupy the landscape (Figure 2-1d).

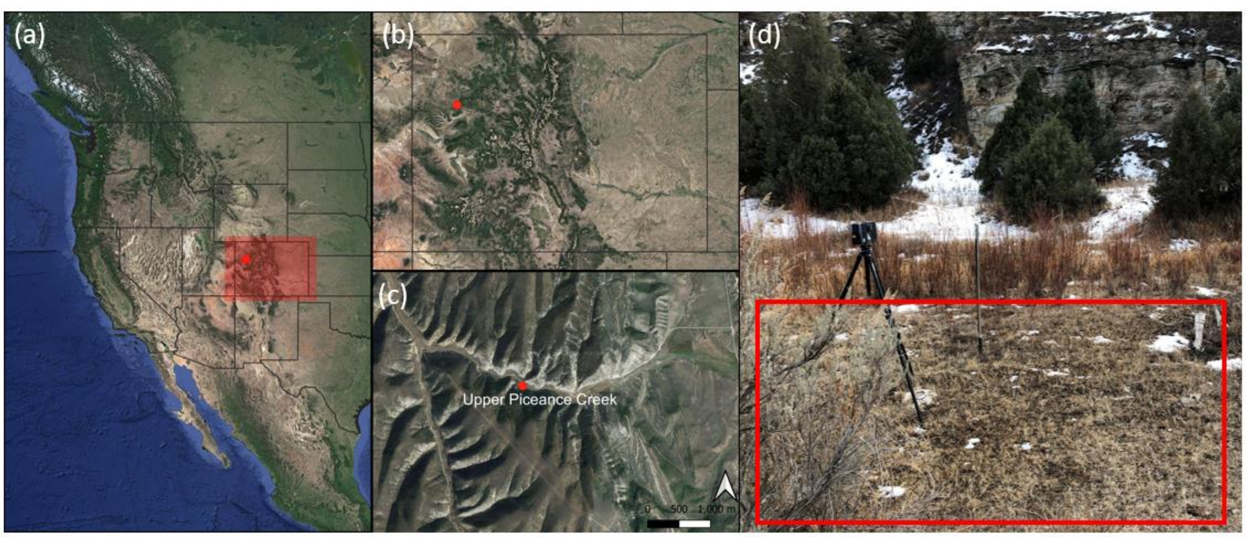

Figure 2-1 a) Location of site within western United States. b) Approximate location of city of Meeker, Colorado on western slope of Rocky Mountains. c) Upper Piceance Creek study site location. d) Upper Piceance Creek study site with Faro terrestrial laser LiDAR scanner in foreground and approximate footprint (red) on 11/15/2019 (photo source: Jessica Sanow).

2.2 Secondary Site: Izas Experimental Catchment

The Izas Experimental Catchment (Alvera et al., 2000) is operated by the Pyrenean Institute of Ecology (IPE) of the Spanish Science Council (CSIC) in Zaragoza, Spain in the headwaters of the Gállego River in the Spanish Central Pyrenees (Figure 2-4a). For this study, the main purpose of this site is to assess the performance of snowfall resurfacing models when applied to hydrologically operational units of significant size and scale. The 55-hectare catchment covers an elevation range from 2056 to 2311 m above sea level and snow depth information (Figure 2-4c). The average winter (Dec through Feb) temperature is 1.2°C with an average winter precipitation total of 750 mm. The predominate land cover consists of subalpine meadows and the lithology is comprised of sandstones and slates (Figure 2-4b). The region is exposed to Atlantic climate conditions associated with relatively humid winters and is characterized by a subarctic climate (Köppen and Geiger subtype Dfc). The snowpack in the catchment typically persists from November until the end of May (Revuelto et al., 2017).

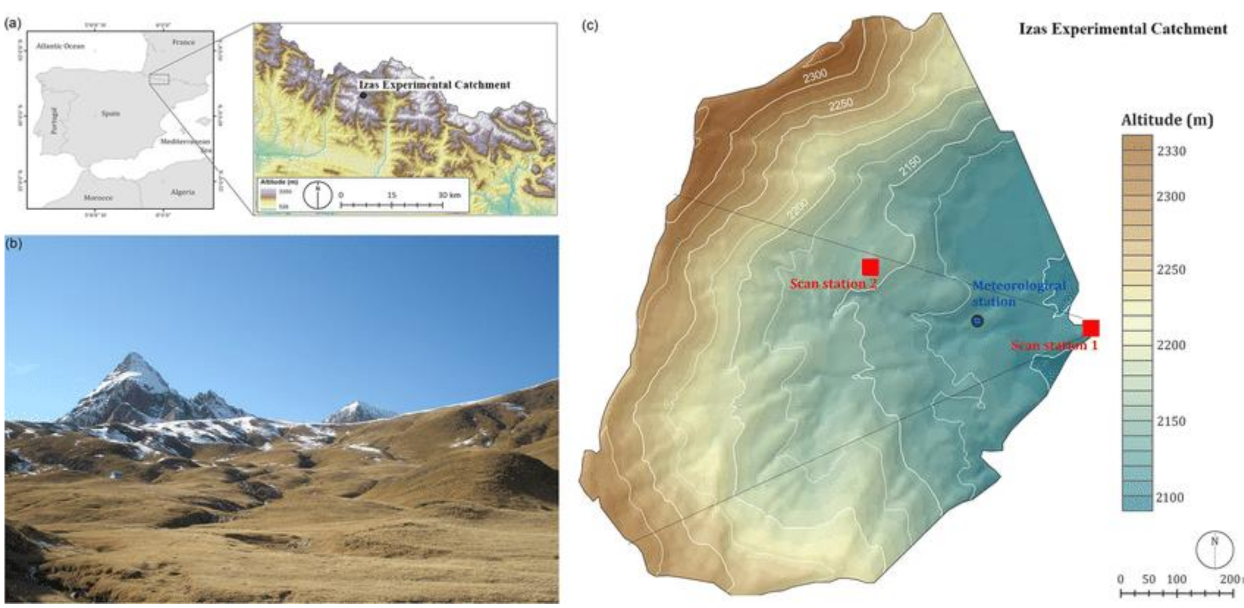

Figure 2-2. a) Izas Experimental Catchment location in the Pyrenees Mountain range in northeast Spain. b) Photo of the catchment showing variable terrain and subalpine meadows. c) Digital elevation model of the catchment with location of meteorological station and TLS scan positions for mapping snow depth (source: Revuelto et al., 2017).

3. METHODS

3.1 Overview of Methodology

This research was performed with the following five sequential steps: data collection, geospatial processing, modeling with machine learning, model sensitivity analysis, and model comparison (Figure 3-1). TLS scans were performed at the UPC field site following snow deposition events, while at Izas, TLS scanning had been conducted previously (Revuelto, 2017). With the CloudCompare software, UPC TLS scans were registered to create a 3D point cloud, ground points were classified using a cloth simulation filter, and then rasterized and exported at 1, 5, and 10 cm resolution digital elevation models (DEM). DEM's from both sites were imported into the QGIS software where they were reprojected and differenced according to the two methodologies (static and dynamic) resulting in gridded snow depth data or rasters. A set of topographic features were calculated from each DEM with Whitebox Tools in QGIS. A machine learning algorithm (XGBoost) was applied to each set of DEM's and used to estimate snow depth from the topographic feature values calculated from the DEM. A sensitivity analysis was performed on each snow depth estimation model to determine model behavior in response to variations in training data size, wind direction, resolution, input extent, feature length, and snowpack phase. The static and dynamic depth estimation models at UPC were then compared by their feature importance distributions and the Nash-Sutcliffe efficiency coefficient. Finally, the snow depth models at UPC were compared to models from Izas Experimental Catchment.

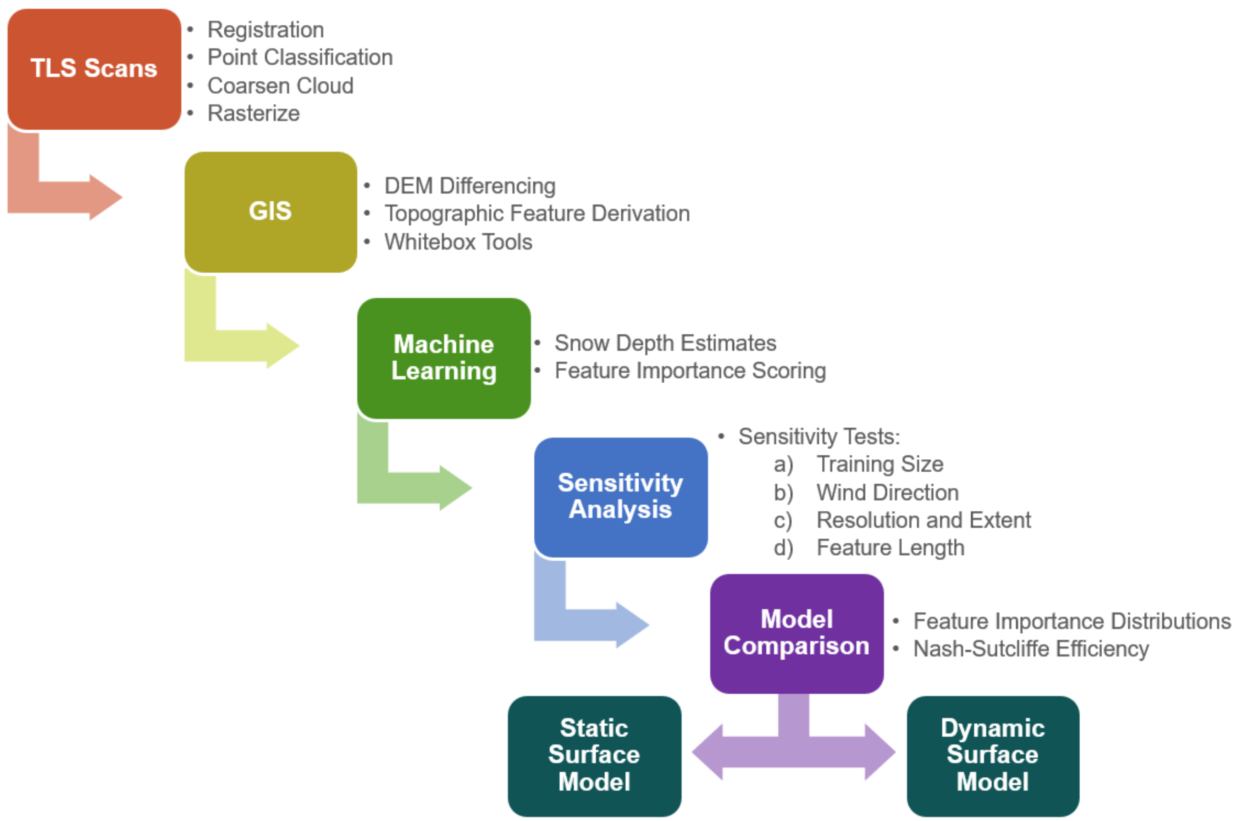

Figure 3-1. General workflow performed in this study. UPC was scanned using a TLS to produce DEM's. The DEM's were used to create topographic features and snow depth rasters in QGIS. A machine learning algorithm was used to estimate snow depth using a static and dynamic surface method. Sensitivity analyses were performed on the models looking at training data size, wind direction, resolution, extent, feature length, and snowpack phase. Finally, the two models were compared using a Nash-Sutcliffe performance metric.

3.2 Data Collection

Data collection consisted of a series of TLS performed at the UPC field site near Meeker, Colorado during the snow season occurring over water year 2020 (10/1/2019 - 9/31/2020). TLS is a ground-based LiDAR method that uses near infrared (1550 nm) pulsed lasers to resolve objects and surfaces at high resolution. A FARO Focus3D X 130 scanner (https://www.faro.com) with a phase-based ranging system was employed after snow deposition events over fixed extent study sites (Figures 2-1d and 3-2a). An integrated global positioning system (GPS) recorded the precise scanner position while the instrument processor resolved incidence angle, time of flight, and return phase resulting in highly accurate location data paired with each return. The scanner was positioned at multiple viewing angles to comprehensively map the snow surface at each site visit. Spherical pylons were placed in each TLS view-scene to aid with scan registration from multiple angles later in processing (Figure 3-2a). UPC was selected for exhibiting high scan frequency, low vegetation obstruction, and variability of the ground surface. An initial TLS scan was performed on 11/15/2019 to capture the snow-free surface characteristics and an additional 8 scans followed while snow was present at the site (Figure 3-2c). The sites were scanned repeatedly over the snow accumulation period with varied frequency based on availability to access the sites after deposition events. A Blue Maestro Tempo Disc™ 3 in 1 sensor (https://bluemaestro.com/) was affixed with a radiation shield and recorded hourly temperature, humidity, and dew point at the site.

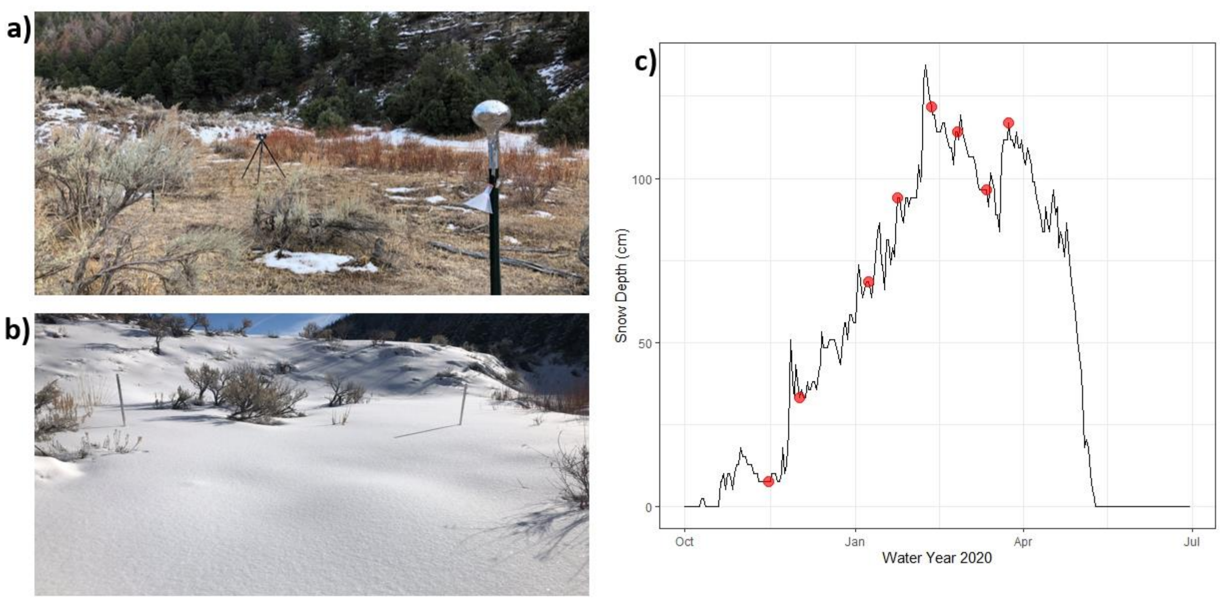

Figure 3-2. a) UPC site near Meeker, Colorado. Faro Focus3D X 130 in background with point cloud registration pylon and BlueMaestro temperature sensor in conical radiation shield in foreground. b) Snow accumulation at UPC scan site on 1/24/2020. c) TLS acquisition dates (red) at UPC shown on snow depth reported at Burro Mountain SNOTEL located approximately 40 kilometers northeast of UPC. The Burro Mountain SNOTEL station is located at 2,865 meters elevation (approximately 700 meters higher than the UPC field site). (Photo credits: J. Sanow)

3.3 TLS Processing

TLS LiDAR processing began with point clouds in CloudCompare version 2.10.2, an open-source three-dimensional processing software (CloudCompare, 2022) in American Standard Code for Information Interchange (ASCII) grid form (Figure 3-1, TLS Scans). Individual TLS scans were registered into a single comprehensive point cloud via the sphere detection method with the Align-point pairs picking tool (Figure 3-3). After the TLS scans were registered, a Cloth Simulation Filter (CSF) plugin feature (Zhang, 2016) was used to classify ground points within the point cloud (Figure 3-4). Settings used for the CSF point classifier are listed in Table 3-1. CSF settings were determined by selecting parameters which removed the highest number of vegetation points within each raw point cloud.

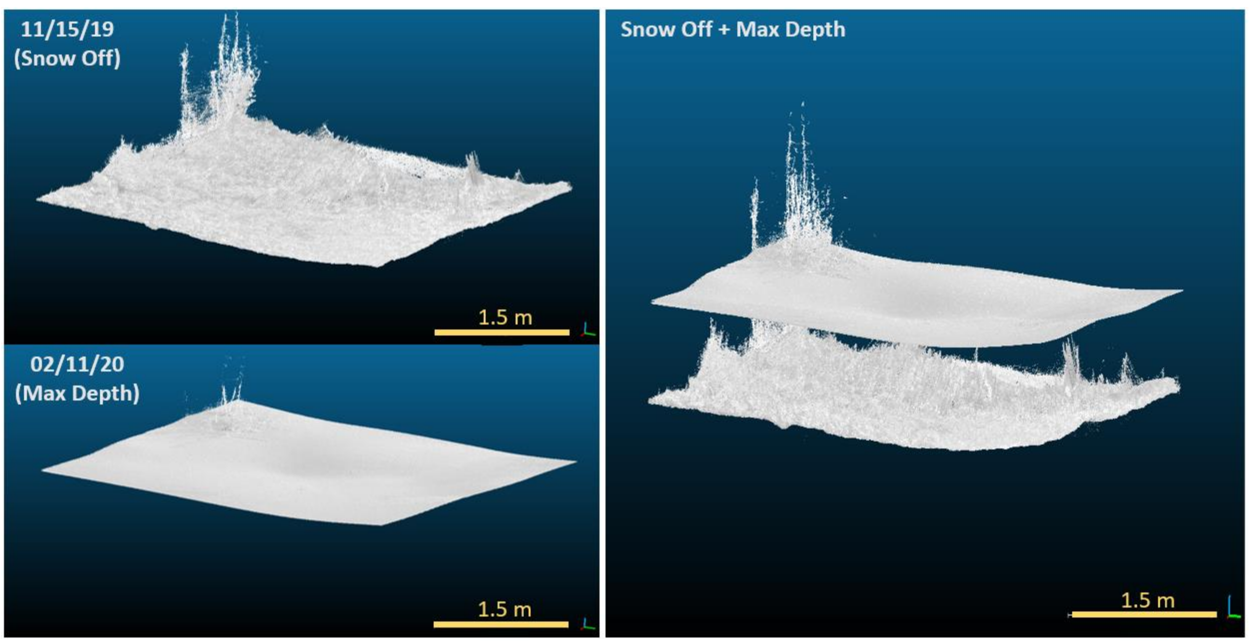

Figure 3-3. Registered point clouds from UPC over the snow accumulation season. Point cloud from no snow scene on 11/15/2019 showing short and medium vegetation (Top Left). Point cloud from max snow depth on 2/11/2020 (Bottom Left). Point clouds displayed simultaneously representing snow off and max snow depth surfaces (Right).

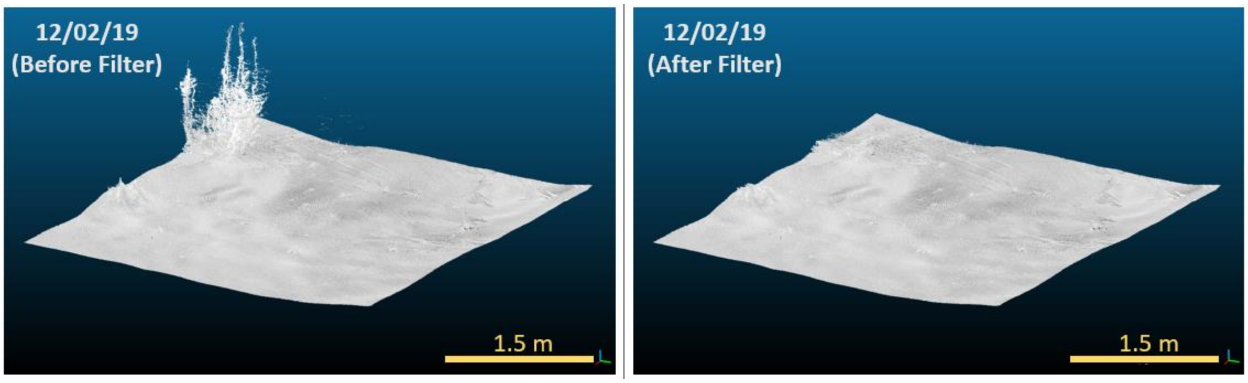

Figure 3-4. LiDAR point cloud at UPC on 12/2/2019 before (left) and after (right) application of Cloth Simulation Filter to classify ground points. In this example, the filter removed approximately 147,000 points or 2.6% of the total LiDAR returns comprising the point cloud.

Table 3-1. Cloth Simulation Filter settings used for classifying ground points in registered Terrestrial Laser Scans. The rigidity of the simulated cloth was controlled by the scene type, while slope processing facilitated a better fit of the simulated cloth to the surface, particularly on steep slopes. Advanced parameter settings for all scans: Cloth Resolution = 0.1m, Maximum Iterations = 1000, Classification Threshold = 0.1m.

Scan Date	Scene Type	Slope Processing Enabled	Vegetation Points Removed	% Points Removed
11/15/2019	Flat	No	170145	2.5
12/2/2019	Relief	No	147013	2.6
1/8/2020	Flat	No	31440	1.3
1/24/2020	Flat	No	15697	0.6
2/11/2020	Steep	No	4749	0.1
2/25/2020	Steep	No	6643	0.2
3/12/2020	Flat	No	60065	1.7
3/24/2020	Flat	Yes	44539	1.3

Once the ground points in each scan were classified, a rasterization tool was applied to create DEM’s at resolutions of 1, 5, and 10 cm. Raster cell elevation values were calculated by taking the mean elevation of all points falling within the bounds of the corresponding grid cell. Raster cells without any LiDAR point returns were given a ‘No Data’ value of -999 to be handled at a later processing stage. DEM’s were then exported in GeoTiff file format for further processing in additional software.

3.4 Raster Processing

The DEM's were imported to QGIS open-source geographic information system software version 3.16.7 (QGIS.org, 2022) for topographic feature creation (Figure 3-1, GIS Processing). Each DEM was assigned a common Universal Transverse Mercator (UTM) projection corresponding to the data collection location using North American Datum 1983, (NAD83 / UTM zone 13N, EPSG:26913). The DEM's were then aligned using a nearest neighbor algorithm. After alignment, elevation derivatives, or topographic features, were calculated with Whitebox Tools, a QGIS plugin consisting of a collection of geospatial analysis tools (Lindsay, 2014). Table 2 lists the topographic features, control group, designators used, parameters, and descriptions from the Whitebox Tools User Manual found in the 'Geomorphometric Processing' sub-toolset. From each DEM, a select series of topographic features were calculated (Figure 3-5). Relative Aspect, Directional Relief, Wind Fetch, and Horizon Angle required a wind direction input parameter which was determined by using the valley direction the UPC site was situated within. Six terrain-based, four wind-based, and four solar-based surface features were derived from each DEM (Table 3-2).

After the topographic features were calculated from each DEM, the DEM's were cropped using the 'Extract by Extent' tool within QGIS. The cropped area was selected to remove edge effects, cell inconsistencies, and regions with large vegetation which resulted in a uniformly sized set of rasters. Finally, the original DEM's were differenced using 'Raster Calculator' with two methodologies to create separate sets of DEM's representing distinct snow depth sets. The first set used the snow-free scan as a constant subtractor where each successive DEM was differenced using the same snow-free DEM and the result represented cumulative snow depth. The second set was differenced using the most recent snow surface DEM and depicted snow depth accumulated between successive site scans.

Table 3-2. Whitebox Tools list applied to LIDAR derived surface DEM's. Descriptions used were taken directly from the Whitebox Tools User Manual (<https://www.whiteboxgeo.com/manual/wbt_book/available_tools/geomorphometric_analysis.html>)

Feature	Control Group	Designator	Settings	Description
Aspect	Solar	Aspect	N/A	Slope orientation in radians clockwise from north based on a polynomial fit of the elevations in a 5x5 neighborhood surrounding each cell.
Circular Variance of Aspect	Solar	CVA	Kernal = 11	Calculates the circular variance (i.e., one minus the mean resultant length) of aspect for an input digital elevation model (DEM). Circular Variance of Aspect is therefore a measure of surface shape complexity, or texture. It will take a value of 0.0 for smooth sites and near 1.0 in areas of high surface roughness or complex topography.
Multi-Directional Hillshade	Solar	Hill	Sun Angle = 45°, revolutions = 360°	Performs a hillshade operation (also called shaded relief) on an input DEM with multiple sources of illumination.
Northness	Solar	North	N/A	Represents northness exposure and is calculated as northness = cosine(aspect) x sine(slope) with units in radians. Northness was not a feature found in the Whitebox Tools and was instead calculated using a raster calculator in QGIS.
Deviation from Mean Elevation	Topographic	DME	Kernal = 11	Calculates the difference between the elevation of each grid cell and the mean elevation of the centering local neighborhood, normalized by standard deviation. This attribute measures the relative topographic position as a fraction of local relief, and so is normalized to the local surface roughness.
Elevation Percentile	Topographic	EP	Kernal = 11, SigFig = 6	Measure of local topographic position (LTP). It expresses the vertical position for a DEM grid cell (z0) as the percentile of the elevation distribution within the filter window.
Mean Curvature	Topographic	MC	N/A	Calculates the mean curvature from a DEM. Mean curvature is the average of any mutually orthogonal normal sections, such as profile and tangential curvature (Wilson, 2018). This variable has an unbounded range that can take either positive or negative values.
Relative Topographic Position	Topographic	RTP	Kernal = 11	An index of local topographic position (i.e. how elevated or low-lying a site is relative to its surroundings) and is a modification of percent elevation range; and accounts for the elevation distribution.
Slope	Topographic	Slope	Units = Degrees	Calculates slope gradient (i.e., slope steepness in degrees, radians, or percent) for each grid cell in an input DEM and is based on a polynomial fit of the elevations within the 5x5 neighborhood surrounding each cell.
Terrain Ruggedness Index	Topographic	TRI	N/A	A measure of local topographic relief. The TRI calculates the root-mean-square-deviation (RMSD) for each grid cell in a DEM calculating the residuals (i.e., elevation differences) between a grid cell and its eight neighbors.
Relative Aspect	Wind	RA	Azimuth = 110	Relative terrain aspect is the angular distance (measured in degrees) between the land-surface aspect and the assumed regional wind azimuth (Bohner and Antonic, 2007). It is bound between 0-degrees (windward direction) and 180-degrees (leeward direction). Relative terrain aspect is the simplest of the measures of topographic exposure to wind, considering terrain orientation only and neglecting the influences of topographic shadowing by distant landforms and the deflection of wind by topography.

Directional Relief	Wind	DR	Azimuth = 110, Max Search = Unlimited	Calculates the relief for each grid cell in a DEM in a specified direction. Directional relief is an index of the degree to which a DEM grid cell is higher or lower than its surroundings. It is calculated by subtracting the elevation of a DEM grid cell from the average elevation of those cells which lie between it and the edge of the DEM in a specified compass direction. Thus, positive values indicate that a grid cell is lower than the average elevation of the grid cells in a specific direction (i.e., relatively sheltered), whereas a negative directional relief indicates that the grid cell is higher (i.e., relatively exposed).
Fetch	Wind	Fetch	Azimuth = 110, Height Increment = 0.01	Creates a new raster in which each grid cell is assigned the distance, in meters, to the nearest topographic obstacle in a specified direction.
Horizon Angle	Wind	HA	Azimuth = 110, Max Search = Unlimited	Calculates the horizon angle (Sx), i.e., the maximum slope along a specified azimuth (0-360 degrees) for each grid cell in an input DEM. Horizon angle is sometime referred to as the maximum upwind slope in wind exposure/sheltering studies. Positive values can be considered sheltered with respect to the azimuth and negative values are exposed. Thus, Sx is a measure of exposure to wind from a specific direction.

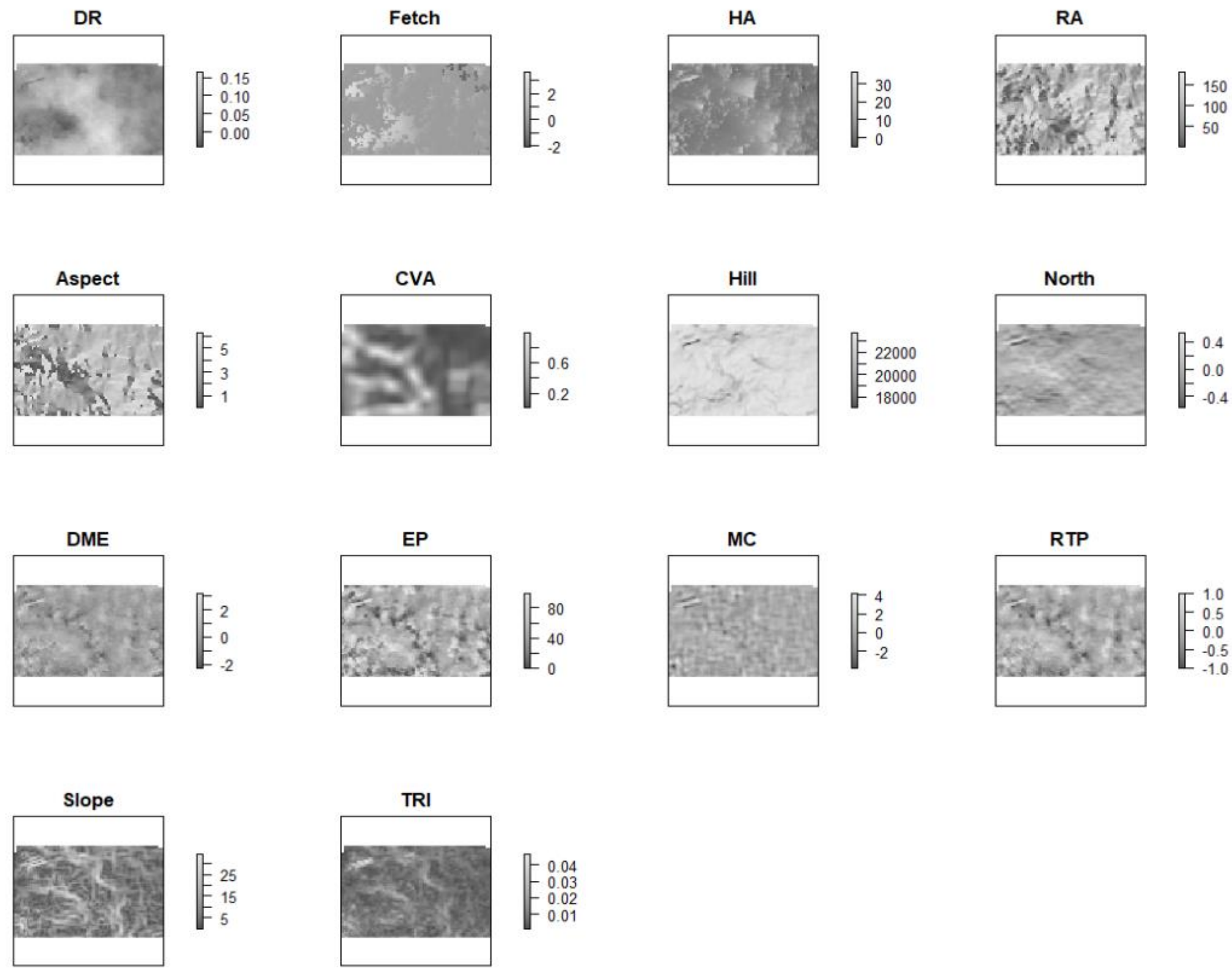

Figure 3-5. Surface features created from LiDAR derived DEM's in QGIS using Whitebox Tools for UPC bare ground surface on 11/15/2019. Table 3-2 summarizes the nature of these features, how they were calculated, and what they represent.

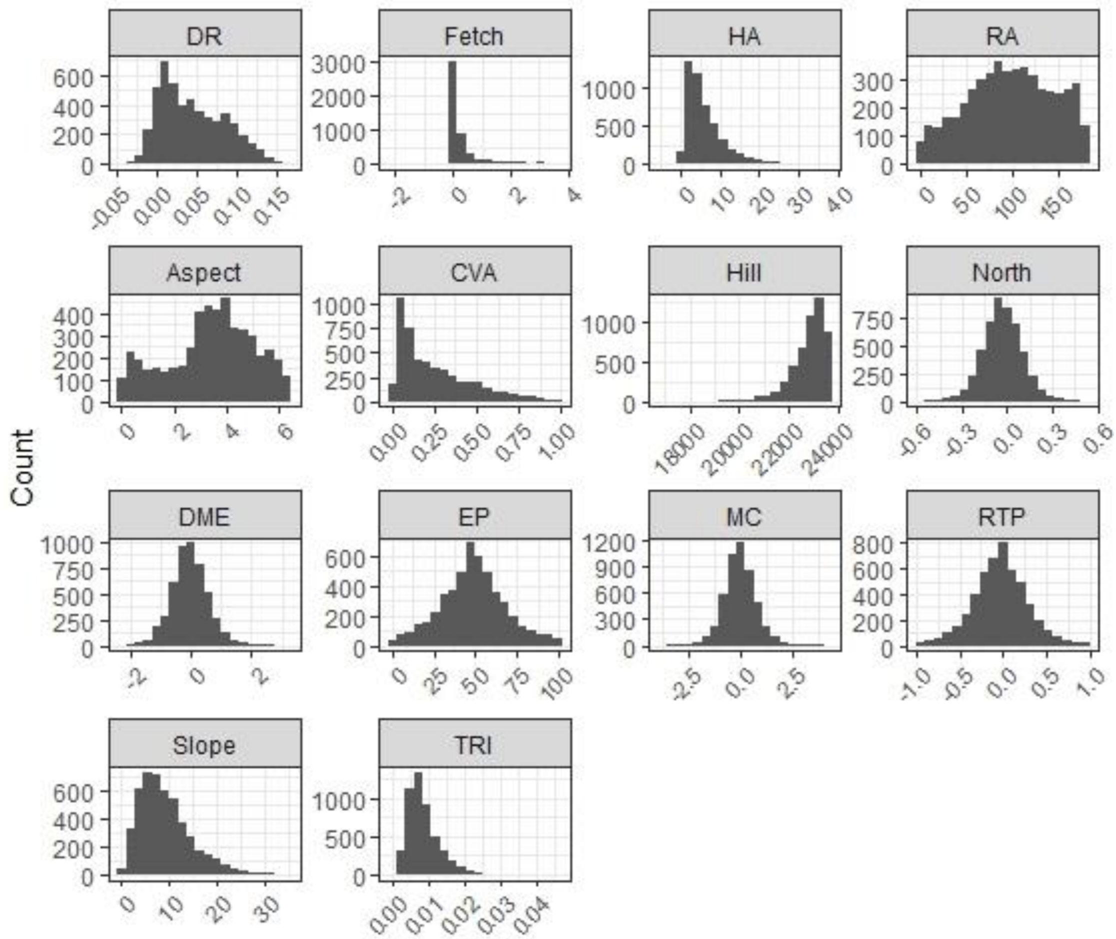

Figure 3-6. Histograms for surface feature rasters displayed in Figure 3-5. Most of the surface features display a normal distribution pattern except for right skewed features: Horizon Angle (HA), Circular Variance of Aspect (CVA), Slope, Terrain Ruggedness Index (TRI) and left skewed: Hillshade (Hill)

3.5 Snow Depth Estimates

The data processing for snow depth estimations was accomplished using R Studio integrated development environment version 3.0.386 (R Core Team, 2023). The topographic features calculated with Whitebox Tools were assembled into a structured dataframe representing each date specific TLS surface scan. The dataframes consisted of grid-cell locations, the associated topographic feature values, and snow depth. Two datasets were created based on the different snow depth derivation methodologies discussed in the following sections.

3.5.1 Snow Depth Estimation Methods

3.5.1.a Static Predecessor

The static predecessor estimation method used topographic feature values (Table 3-2) from the snow-free DEM to make estimates of snow depth and the resulting snow depth estimates represent the cumulative seasonal snow depth at the time of estimation (Figure 3-6a). The method is termed “static” due to the unchanging nature of the surface feature parameters used to estimate snow depth.

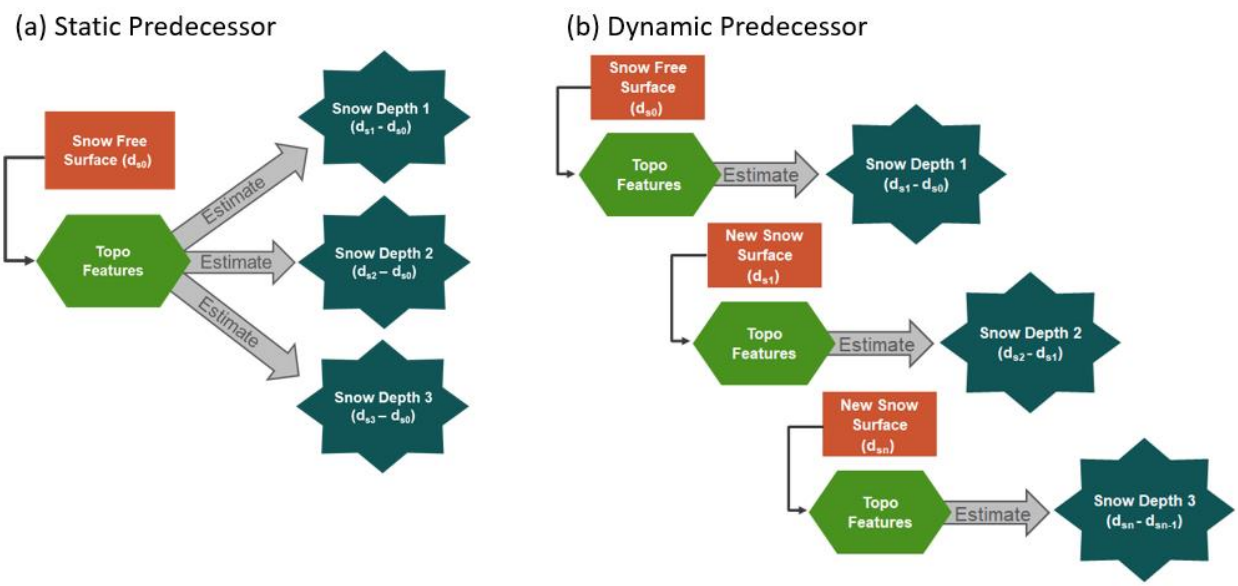

Figure 3-2. (a) Representation of static predecessor snow depth estimation methodology. Topographic features are calculated from the initial snow free surface DEM and used in the model to estimate total snow accumulated at each DEM grid cell. (b) Representation of dynamic predecessor estimation methodology. Topographic features are calculated from each new snow affected surface and used in the model to estimate incremental snow depth.

3.5.1.b Dynamic Predecessor

A second method called dynamic predecessor was used for making additional snow depth estimates. This method differed from the static predecessor such that topographic surface feature values were recalculated at each timestep to reflect the changes brought about by the new snow (Figure 3-6b). The snow depth estimates from the dynamic predecessor method are more representative of natural processes and characterize the snow depth change between successive site visits.

3.5.2 Machine Learning

A widely implemented machine learning algorithm called XGBoost (Chen et al., 2016) was used to estimate snow depth via the dynamic and static predecessor methodologies (Figure 3-1, Machine Learning). This algorithm in part derives its name from gradient boosting, which is a machine learning technique that employs an ensemble of weak prediction models in the form of decision trees to make accurate predictions (Figure 3-7). This class of algorithm can be an effective tool for regression and classification problems with structured data and is recognized for its accuracy, efficiency, and feasibility (Alshari et al., 2021).

Feature importance serves as a descriptive tool that quantifies the significance of individual model inputs in the construction of regression trees, ultimately contributing to the estimates. A feature exhibiting high relative importance is more effective at splitting the target variable and building trees, while a low relative importance indicates a poor target splitter and tree builder. In the XGBoost model, feature importance is closely related to the gain metric which represents the improvement in the model's performance achieved by splitting on an individual feature. The gain for a particular split is calculated by combining the scores of the left and right leaf nodes at the split and the difference between the combined score and the sum of the scores of the individual leaves. Feature importance quantifies the contribution each feature makes to the overall performance of the model and is calculated as the sum of the gains for each individual feature for every split in the ensemble model. The feature importance is represented in a relative manner, where the aggregate of all feature importance equals 1.

To begin the process, 80% of each dataset was randomly partitioned for training a model and the remaining 20% for testing the performance. The machine learning model was trained to estimate snow depth at each grid cell using the DEM derived surface feature values as parameters. The grid-cell locations were excluded to prevent spatial autocorrelation. The machine learning model was configured with a tree-based linear regression objective which attempts to minimize root mean squared error (RMSE) of the residuals of the model with the observed snow depths. Each trained model was tasked with iteratively constructing regression trees until three consecutive iterations resulted in no further reduction in RMSE. Furthermore, a maximum leaf depth of 6 was maintained throughout the process. All other model parameters related to tuning were left on the default setting for simplicity, uniformity, and ease of comparison purposes. Model parameter hyper-tuning was not performed given that model consistency was preferred in-lieu of individual optimization. After the models were tested, the importance values for each topographic feature were recorded along with mean absolute error, mean standard error, and RMSE.

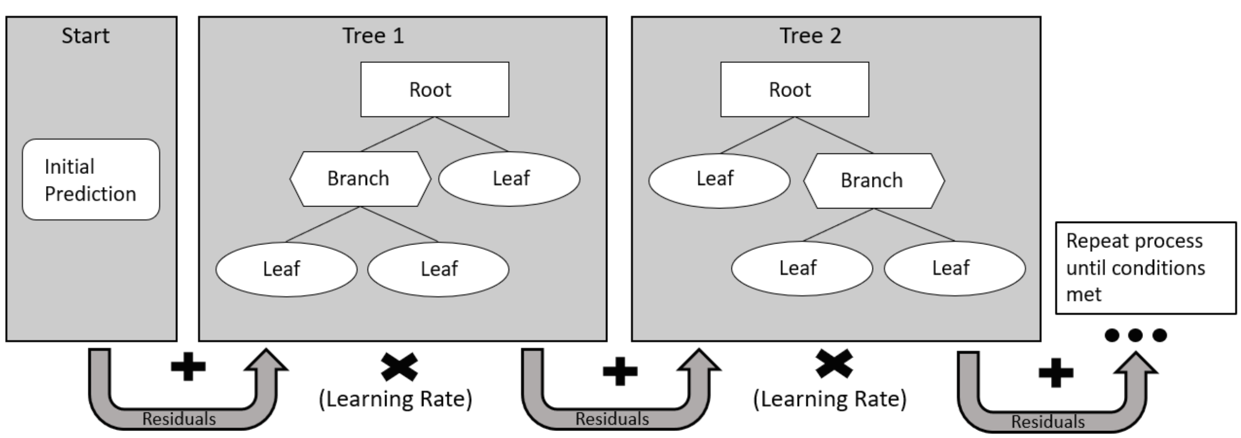

Figure 3-7. Simplified process diagram of XGBoost gradient boosting machine learning. The process starts with an initial prediction. Residuals are computed and used to construct a decision tree. At each branch or node of the tree, the feature and threshold that maximize the gain are selected for the split. Output values are calculated for each

leaf of the tree based on the residuals and become the new residuals for the dataset. This process is repeated, with each subsequent tree learning from the residuals of the previous tree and adjusting its predictions. The process continues until the residuals stop reducing or until a specified condition is met.

In XGBoost, the process begins with an initial prediction of the target variable where prediction residuals are computed and used to construct a decision tree. At each branch or node of the tree, a similarity score is calculated for the residuals and the feature and threshold that maximize the gain in similarity are assigned to the split. The residual similarities in each leaf are evaluated along with the similarity gain from the next split. By comparing the gains, the algorithm determines the feature and threshold that provides the most valuable information for predicting the target variable. The output value for each leaf is calculated based on the residuals. This process is repeated iteratively, with each subsequent tree learning from the previous residuals and adjusting its predictions accordingly. The iterations continue until the residuals stop reducing or until a specified number of iterations is reached. The model assigns higher weight to the trees that contribute more to the overall performance rather than equal weights like in other related algorithms. Finally, the concluding prediction is made via the aggregate of the predictions from all the trees with their associated weights. This approach allows XGBoost to gradually improve its predictions by learning from the estimate residuals and incorporating the information gained from each tree.

3.6 Sensitivity Analysis

A sensitivity analysis of the UPC snow depth estimation models was conducted to see how the models behaved in response to changes to the inputs (Table 3-3). A base case model consisting of 80% training data, 5 cm resolution, 110° wind direction, cropped extent, and trimmed feature length was established to appropriately perform the tests. Directional Relief was identified in the initial model as a topographic feature of interest (TFOI) and used to indicate the effect on the model. The models were first subjected to changes in the size and selection method of the original dataset that was allocated for training, and the response in the RMSE of the model estimates with the testing data were tracked. The following sensitivity tests measured changes in the TFOI as the determination of effect. First, wind direction was varied 30° and 60° to either side of the existing valley azimuth of 110°. Next, the resolution of the DEM's and resulting topographic features was changed to 1 and 10 cm. The extent of the input DEM varied between a full range which included vegetated areas that persisted through the CSF and a cropped extent which was focused on an unobstructed region of the point cloud. Feature lengths varied between a full set which included all 14 of the topographic features and a trimmed set which consisted of only the features that exhibited a feature importance of greater than 0.1 at least once over the observation period. Finally, the snowpack was classified into either an accumulation or net loss state determined by the average change in snow height.

Table 3-3. Summary of sensitivity tests performed, and the attributes tested on the snow estimation models at UPC. To perform the analyses a base case model consisting of 80% test data, 110° wind direction, 5 cm resolution, cropped extent, and a trimmed feature length were used with directional relief as an indicator feature where appropriate.

Sensitivity Test	Attribute Tested
Training Size	70-90%
Wind Direction	50, 80, 110, 140, 170°
Resolution	1, 5, 10cm
Extent	Full, Cropped
Feature Length	All, Trimmed
Snowpack Status	Accumulation, Net Loss

3.7 Model Comparison

The Nash-Sutcliffe Efficiency (NSE) index was calculated for each snow depth estimation method and used to evaluate model performance within and between the sites (Nash and Sutcliffe, 1970) (Figure 3-1, Model Comparison). NSE is normally used to assess the predictive ability of hydrological models and is defined by (Eq. 3-1). In a perfect model, where estimation error variance equals 0, the NSE will result in a score of 1. When NSE equals zero (the estimation error variance equals the variance of the observed time series), the model has the same predictive ability as the mean of the time series. A score of less than zero indicates the mean of the time series serves as a better predictor than the model and, in general, model simulation can be judged as satisfactory if NSE > 0.50 (Moriasi, et al., 2007).

$$NSE = 1 - \frac{\sum_{t=1}^{T}(Q_0^t - Q_m^t)^2}{\sum_{t=1}^{T}(Q_0^t - \bar{Q}_0)^2}$$

(Eq. 3-1)

NSE coefficients were calculated for both the static and dynamic snow depth estimation models at both the UPC and Izas Experimental Catchment sites. These coefficients, along with the feature importance distributions provided by the machine learning model, were utilized to compare the performance of the static and dynamic models within each site as well as between the two sites.

4. RESULTS

4.1 Model Behavior Assessment

To frame the investigation of the nature of the model and more easily make comparisons, a base case model was established for the UPC dataset consisting of an extent cropped 5 cm DEM origin (Table 3-3). A resolution of 5 cm was selected on the basis that it was the middle of the three resolutions evaluated and an edge cropped DEM focused on the center of the LiDAR scene which omitted large vegetation intrusions that persisted through the cloth simulation ground point filter. From the base case, Directional Relief was selected as a feature of interest to illustrate differences between the static and dynamic snow depth estimation models because it had a feature importance greater than 0.6 for at least one observation using both approaches (Figure 4-1c).

4.1.1 Base Case Time Series

Snow depth at the UPC site was calculated from each TLS scan using the static predecessor method (Figure 4-1). Snow depth variability was apparent in the first scan (12/2/2019) and relative snow depth patterns emerge beginning at the following site visit (1/8/2020) where a deeper snow depth band appears between two relatively shallower zones. This snow depth variability pattern remains relatively consistent through the accumulation period (12/2/2019 – 2/25/2020) and remains during the net loss period as well (3/12/2020 – 3/24/2020).

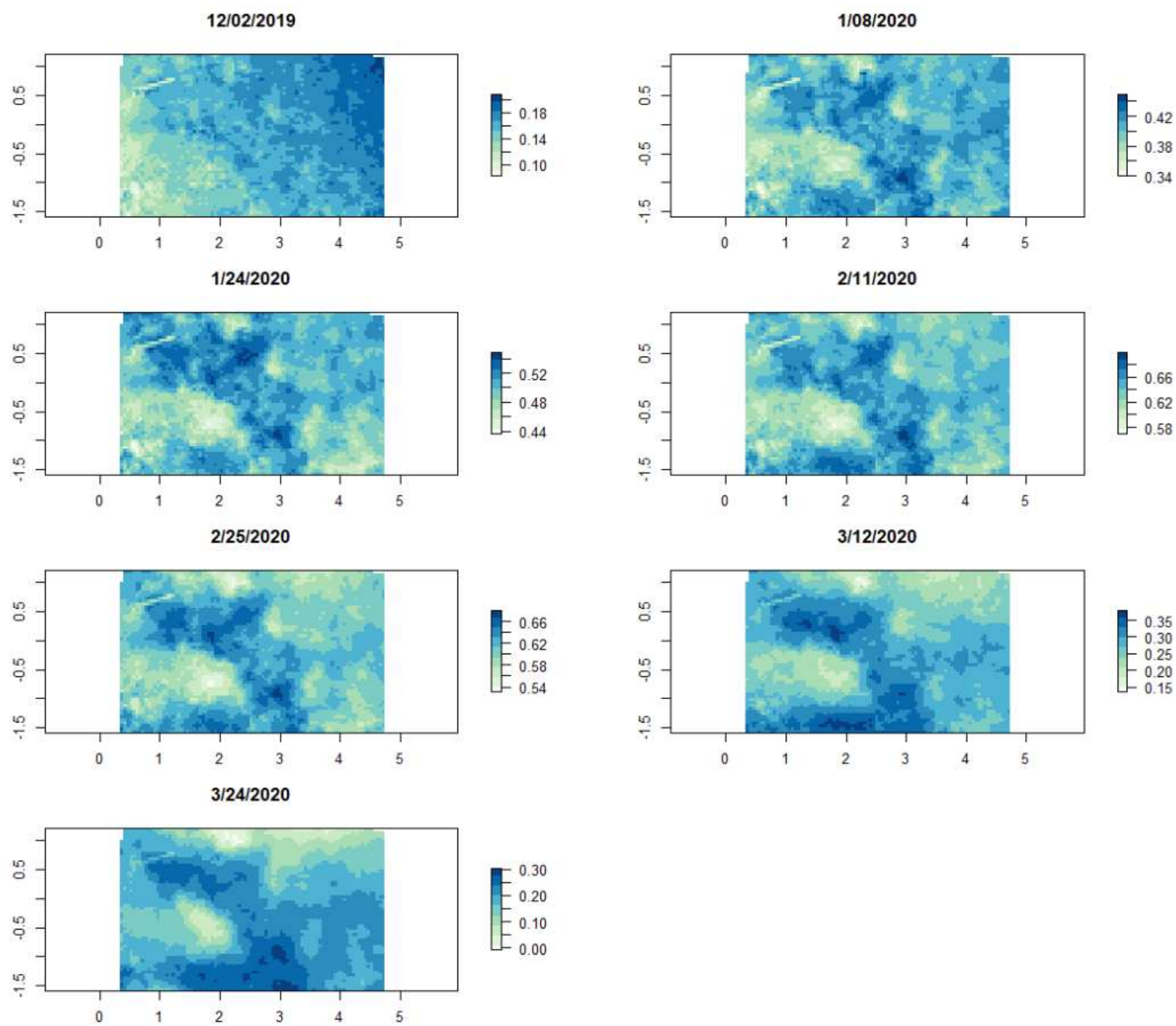

Figure 4-1. Snow accumulation patterns at UPC (5 cm resolution, cropped) over the sampling period using the static surface differencing method with snow depths measured in meters. As the accumulation season progressed, snow depth patterns emerged with zones of consistently deeper snow (darker blue) as well as regions of relatively shallower snow.

Examining the feature importance over the sampling period, the static depth estimation model resulted in high importance scores for Directional Relief (DR), Relative Topographic Position (RTP), and to a lesser extent Circular Variance of Aspect (CVA) (Figure 4-2). Early in the accumulation period, RTP had the highest importance, but as the season progressed DR importance increased inversely with RTP. During the end of the sampling period, DR displayed a small decline that was supplanted by an increase in CVA importance. Overall, these three topographic features account for most of the total importance within the static estimation model. The dynamic snow depth model found Aspect, CVA, DR, Fetch, Horizon Angle (HA), Multi-Directional Hillshade (Hill), Mean Curvature (MC), Northness (North), Relative Aspect (RA), and RTP all to be at least momentarily important estimators (Figure 4-2). DR was the highest source of importance over the observation period. The behavior of the feature importance in the dynamic model is characterized by a flashy nature.

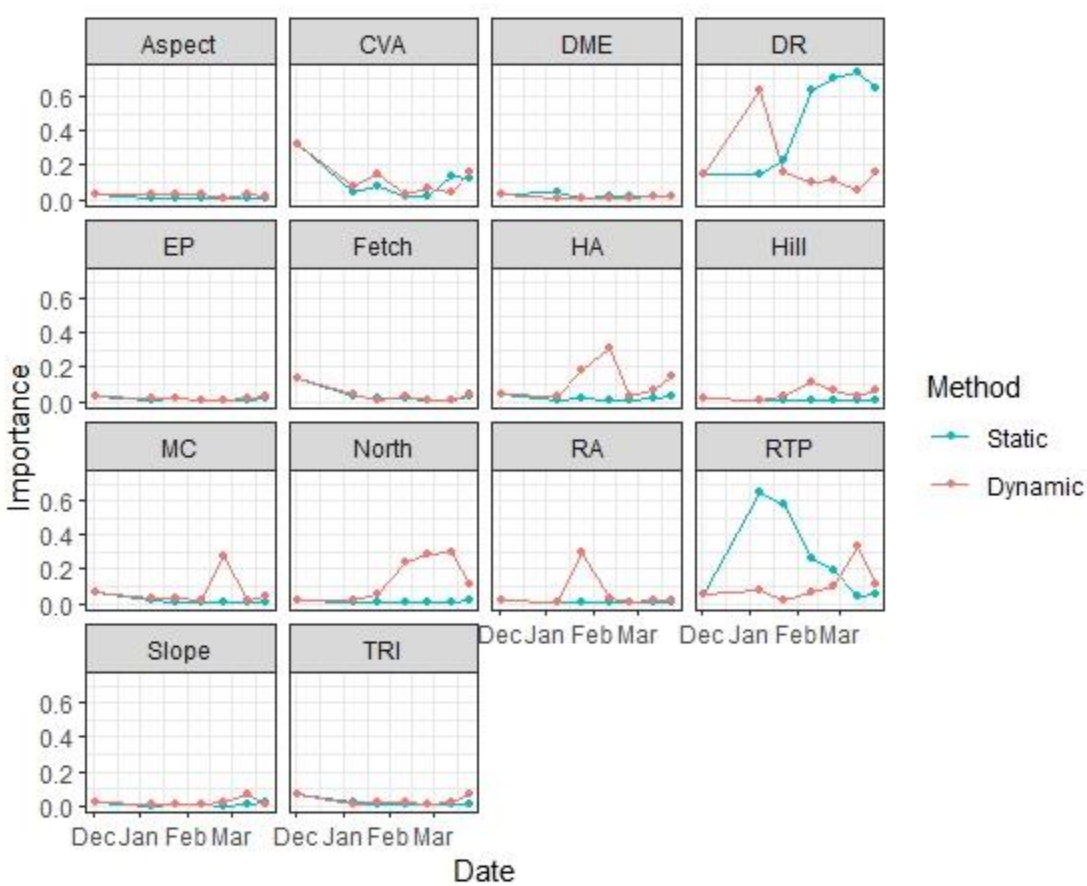

Figure 4-2. Base case (5 cm, cropped) individual feature importance time series for all topographic features computed for the static and dynamic snow estimation method. The static method feature importance is concentrated on Directional Relief (DR) and Relative Topographic Position (RTP). The dynamic method feature importance was comprised of more features including: Circular Variance of Aspect (CVA), DR, Horizon Angle (HA), Mean Curvature (MC), Northness (North), Relative Aspect (RA), and RTP.

The Directional Relief for the initial bare ground scan (11/15/2019) shows a distinct pattern with a sheltered (positive values) circular-like structure formed with exposed zones (negative values) on the center-left side and to a lesser extent in the upper-right (Figure 4-3). As snow was deposited over the season (12/2/2019 – 2/25/2020) the inherent Directional Relief pattern persisted but the distinction between the exposed and sheltered zones became increasingly muted, i.e., the surface was smoothed. As net loss proceeded (3/12/2020 – 3/24/2020), the prevailing directional exposure structure was decomposed and gave way to the emergence of a new pattern as the snowpack receded.

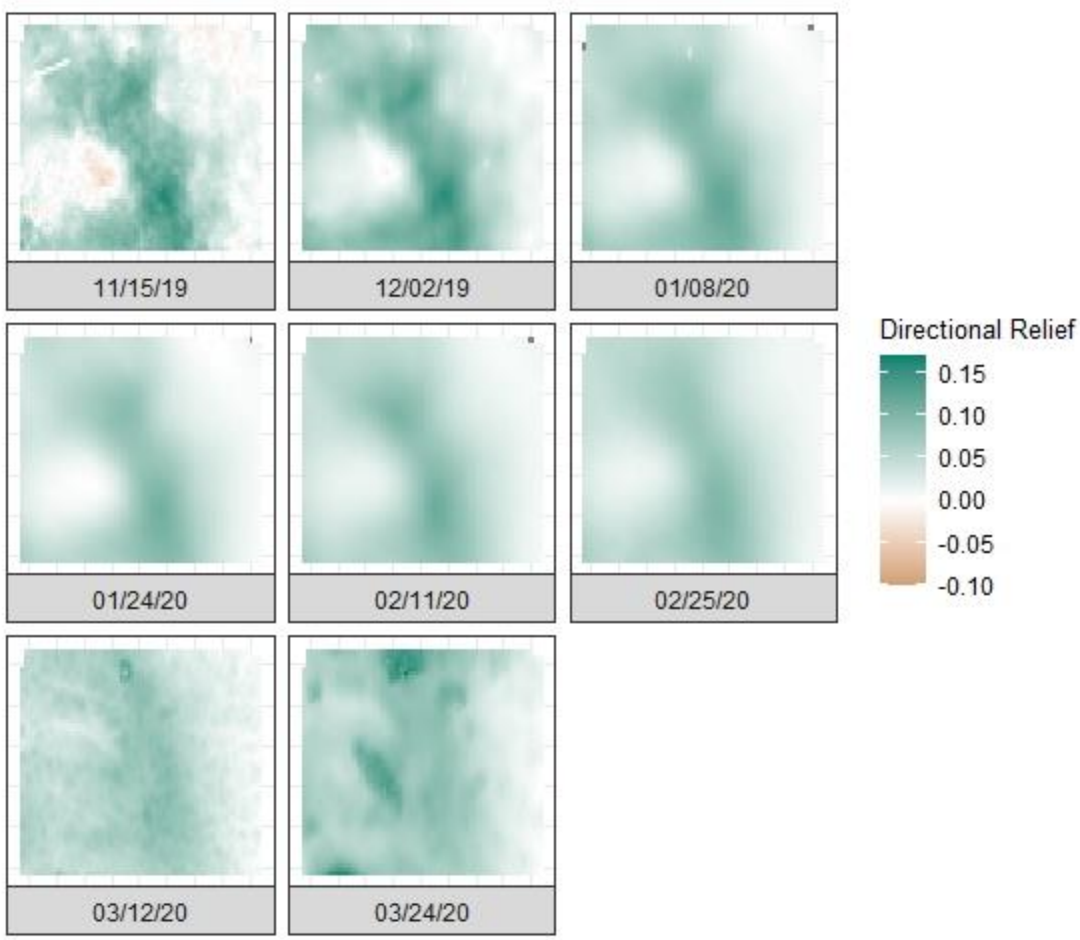

Figure 4-3. Directional Relief depicted from each TLS scan for the duration of the collection period at the UPC site. Bare ground scene represented on 11/15/2019. Snow accumulates at the site starting on 12/02/2019 and ending on 2/25/2020. Net loss of snow depth becomes prevalent on 03/12/2020 through 03/24/2020. Positive values relatively sheltered regions and negative values indicate relative exposure.

4.1.2 Sensitivity Analysis

The training data percentage supplied to build the depth estimation models was adjusted from 70-90% in 10% increments and two distinct partitioning methods were used to observe the effect on the model estimates (Figure 4-4). The contiguous selection method resulted in decreased RMSE for both methods of snow depth estimates as the supplied training data size was increased. The static model had a lower median RMSE than the dynamic model but had wider IQR's and minimum-maximum ranges of RMSE distributions. Randomly selecting the testing partition resulted in minor changes in RMSE distributions for both models regardless of the training size allocated and the dynamic model produced lower RMSE distributions than the static model. Compared by partition type, the random selection method outperformed the contiguous method when training data supplied was less than 90% of the available dataset.

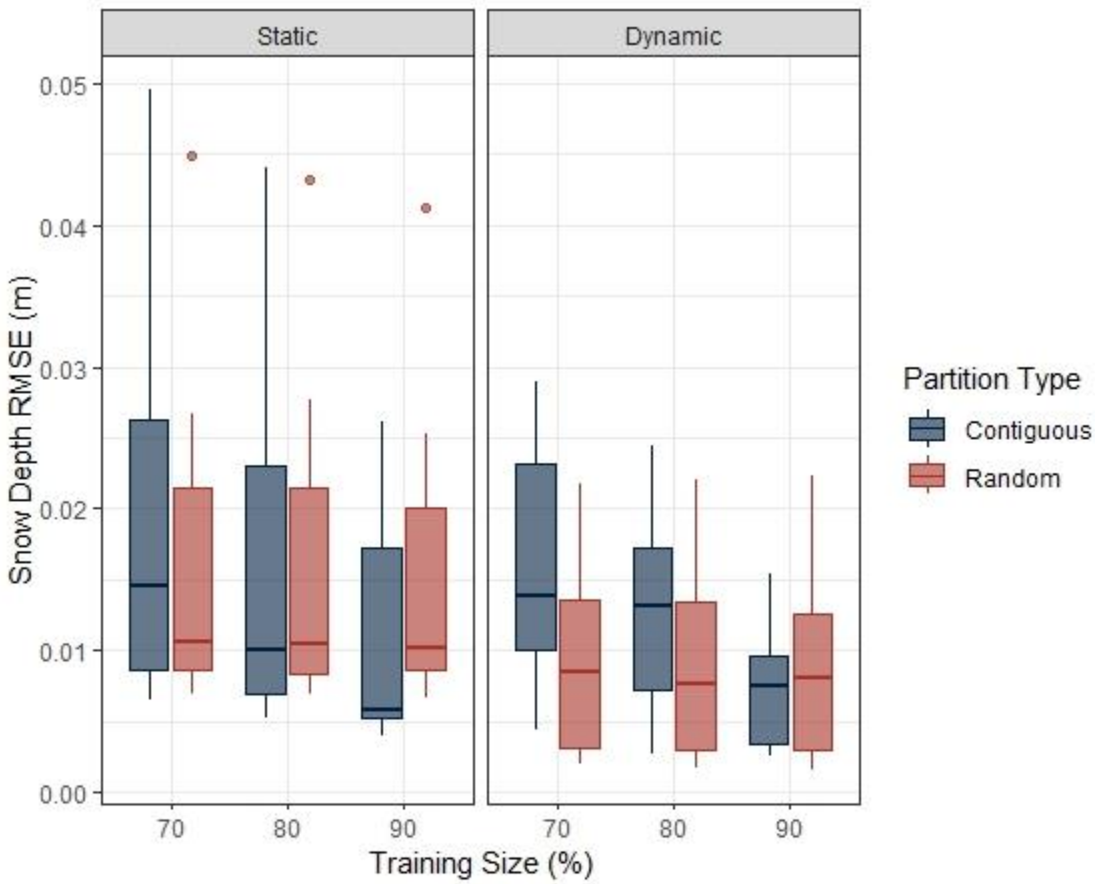

Figure 4-4. Training data partition and selection method sensitivity analysis for static and dynamic models. Changes to the amount of the training data supplied affected the contiguous selection method more than the random sample method with decreasing root mean squared error (RMSE) of snow depth estimates as the training partition was increased. The random sample method was more resilient to changes in the size of the training partition in both the static and dynamic methods.

The wind direction used to create Directional Relief was varied from the UPC valley azimuth (110°) by 30° and 60° on either side and the feature importance was calculated using each method (Figure 4-5). The static method resulted in higher importance toward the end of the observation period and the directions used followed a similar pattern except for the third observation (1/24/2020) where directions of 50° and 80° resulted in high feature importance whereas the rest of the directions cause low feature importance. The dynamic method was less ordered, and a direction of 110° resulted in high importance at the second observation (1/8/2020) which decreased for the remainder of the observations. The other directions tested produced mostly low feature importance scores with 80° and 170° wind directions resulting in the highest importance at various points on the timeline.

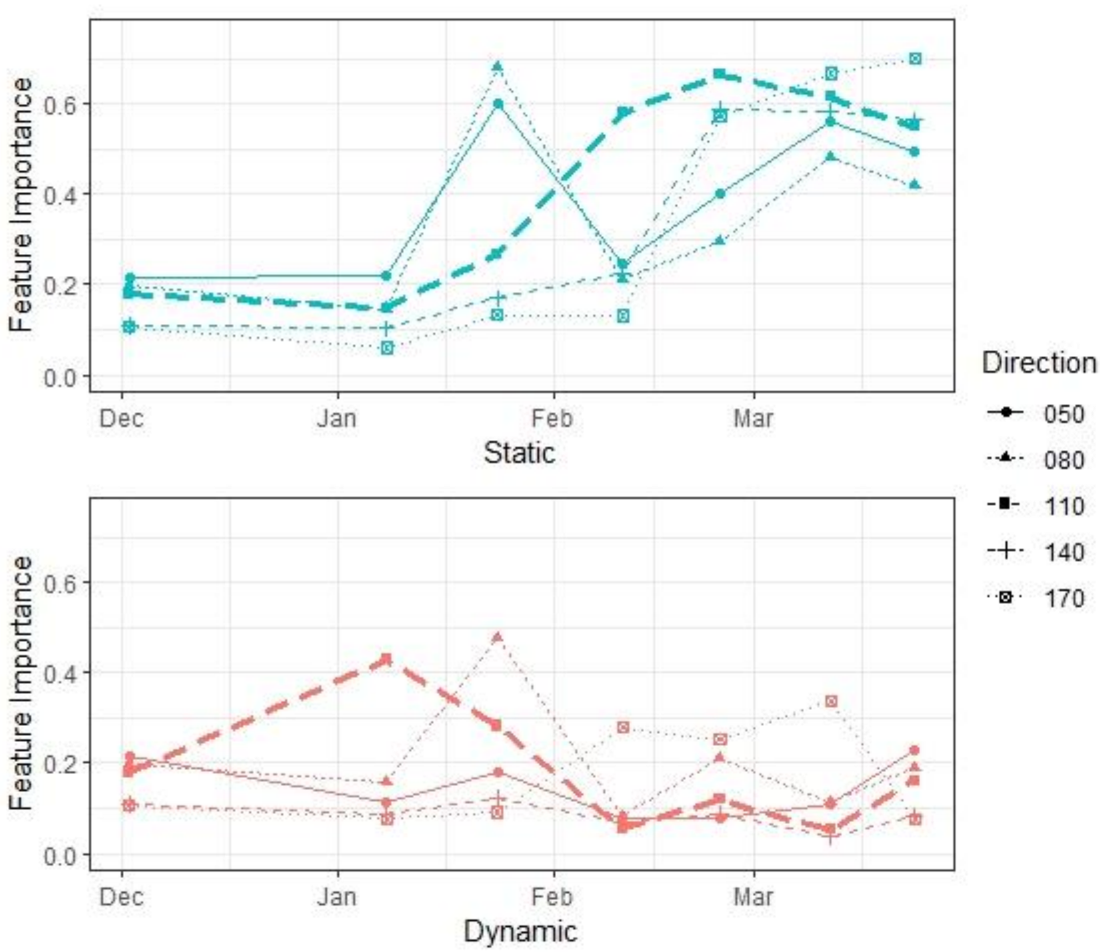

Figure 4-5. Directional Relief feature importance for the various wind directions tested separated by estimation method. The importance of Directional Relief to the depth estimates depends on the wind direction used in the feature creation for both the static and dynamic models. The importance for the wind direction of 110 degrees (valley direction) has been bolded for both methods.

With the static method, Directional Relief initially showed low importance but increased throughout the season reaching peak in late February (Figure 4-6a) as input resolution was varied. The 1 and 5 cm models displayed rapid increases in importance whereas the 10 cm model displayed a more gradual increase in importance. The dynamic method exhibited a sharp increase in feature importance scores upon the addition of snow, followed by a rapid decline back to near-initial values. Representing the snow surface at finer resolutions resulted in higher Directional Relief importance for both methods with larger differences over the sampling period occurring from the static method.

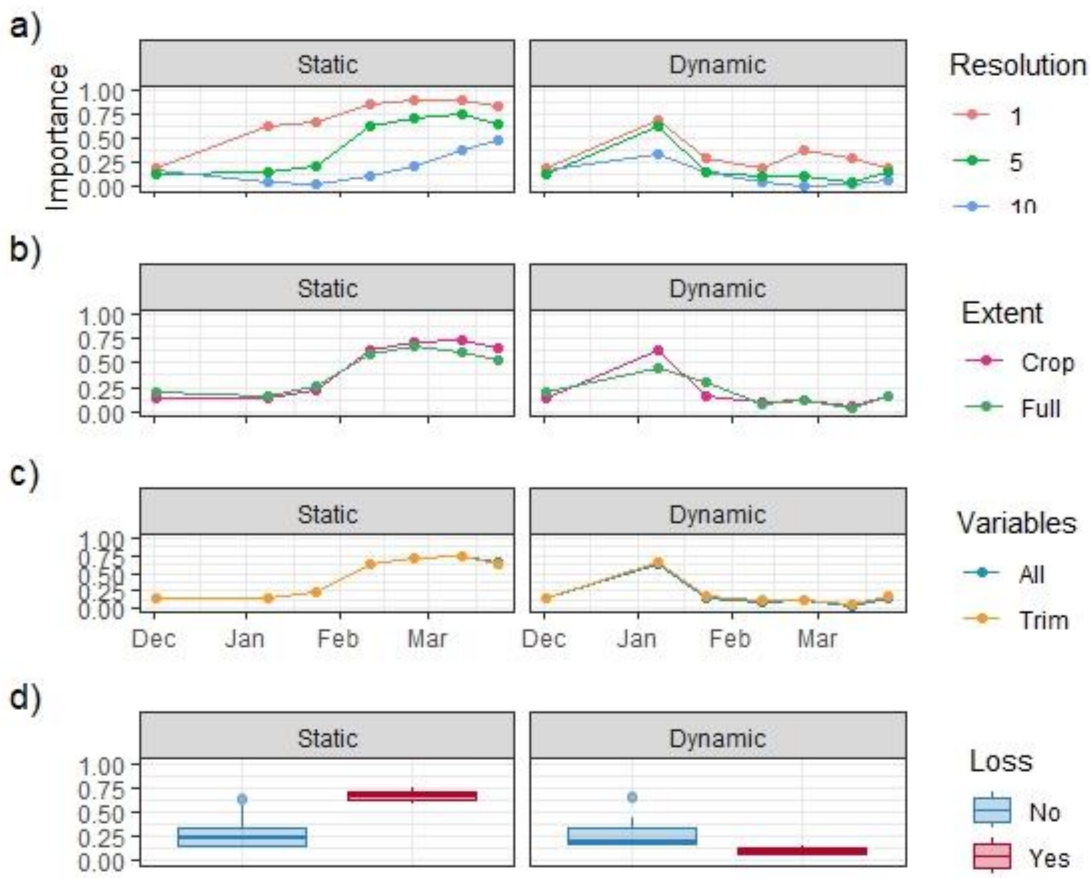

Figure 4-6. Sensitivity analysis illustrated using Directional Relief. a) Static and dynamic method Directional Relief feature importance for 1, 5, 10 cm resolutions, b) Static and dynamic method Directional Relief feature importance for cropped and full extent DEM's, c) Static and dynamic method Directional Relief feature importance for trimmed and full topographic feature lengths, d) Static and dynamic method Directional Relief feature importance for accumulation period vs. net loss period.

There was some difference in the feature importance for the full extent model compared to the cropped model, with the largest difference in the static model occurring at the end of the sampling and near the beginning for the dynamic model (Figure 4-6b). Where deviation occurred in the static model the cropped extent resulted in higher importance. The dynamic model varied between having higher importance resulting from the cropped extent and the full extent. For both models, the difference in directional relief importance related to the extent used was marginal.

From the static method, Directional Relief was nearly unaffected using a trimmed topographic feature length with the largest difference occurring at the end of the observation period (Figure 4-6c). The dynamic method was similarly unaffected by the length of the feature set. When the Directional Relief feature importance was evaluated during the accumulation period (n=16) versus the net loss period (n=12), the static method yielded lower feature importance from the accumulation phase (Figure 4-6d). For the dynamic method, the accumulation phase (n=16) resulted in higher Directional Relief importance than the net loss phase (n=12). The distributions of accumulation phase importance were wider than net loss distributions for both methods.

4.2 Evaluation of Accumulation Models

4.2.1 Feature Importance Basis

When importance scores less than 10% were withheld, the static model (n=174) had a higher median (static = 0.28, dynamic = 0.16), wider IQR, and higher maximum importance than the dynamic method (n=288) (Figure4-7a). When the distributions were grouped by the tested resolutions, the static method distributions resulted in higher medians, wider IQR's, and higher maximum ranges than the dynamic method in each case (Figure 4-7b). For the static method, the 10 and 5 cm resolutions lead to similar importance distributions while the 1 cm resolution resulted in an increased median, IQR, and maximum range. Resolution changes affected the dynamic method importance distributions less, and resulted in several more outlying high importance observations as resolution was increased from 10 to 1 cm.

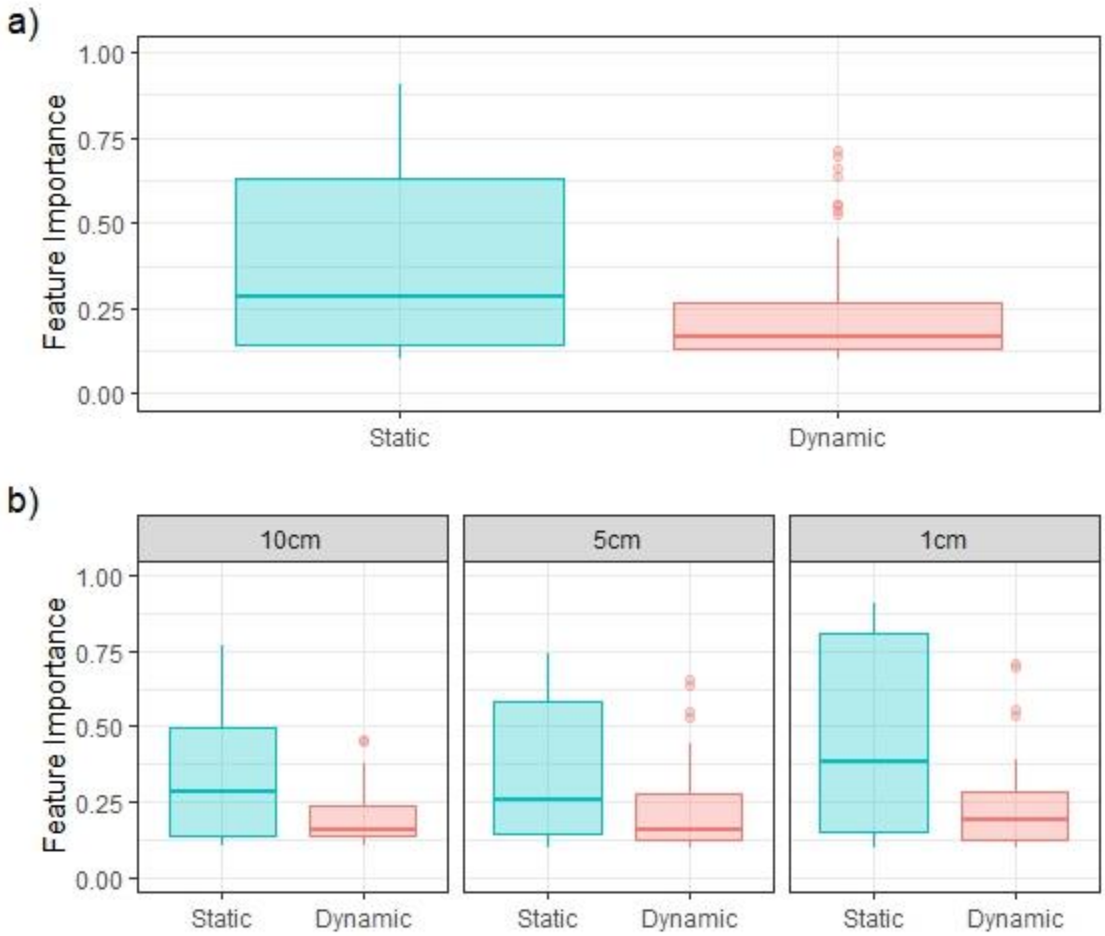

Figure 4-7. a) Feature importance distributions for static and dynamic methods after removal of low importance features (importance < 0.1). The static method results in wider distributions of feature importance with higher medians. When resolution is increased, the feature importance distribution and median increases while the dynamic method was less affected.

4.2.2 Topographic Feature Importance Distributions

When importance scores of less than 0.1 were withheld from all model combinations, the static method was overwhelmingly influenced by Directional Relief (highest median and maximum importance) and Relative Topographic Position (Figure 4-8). Only three additional topographic features (CVA, EP, and TRI) made contributions higher than 0.25 and a total of 8 features registered importance values above the threshold over the sampling period. The dynamic model features with the highest contribution to depth estimates were Directional Relief, Northness and Relative Aspect. These three features had narrower distributions than the high influence features from the static model. Throughout the dynamic model timeline, 13 topographic feature sources contributed to the snow depth estimates.

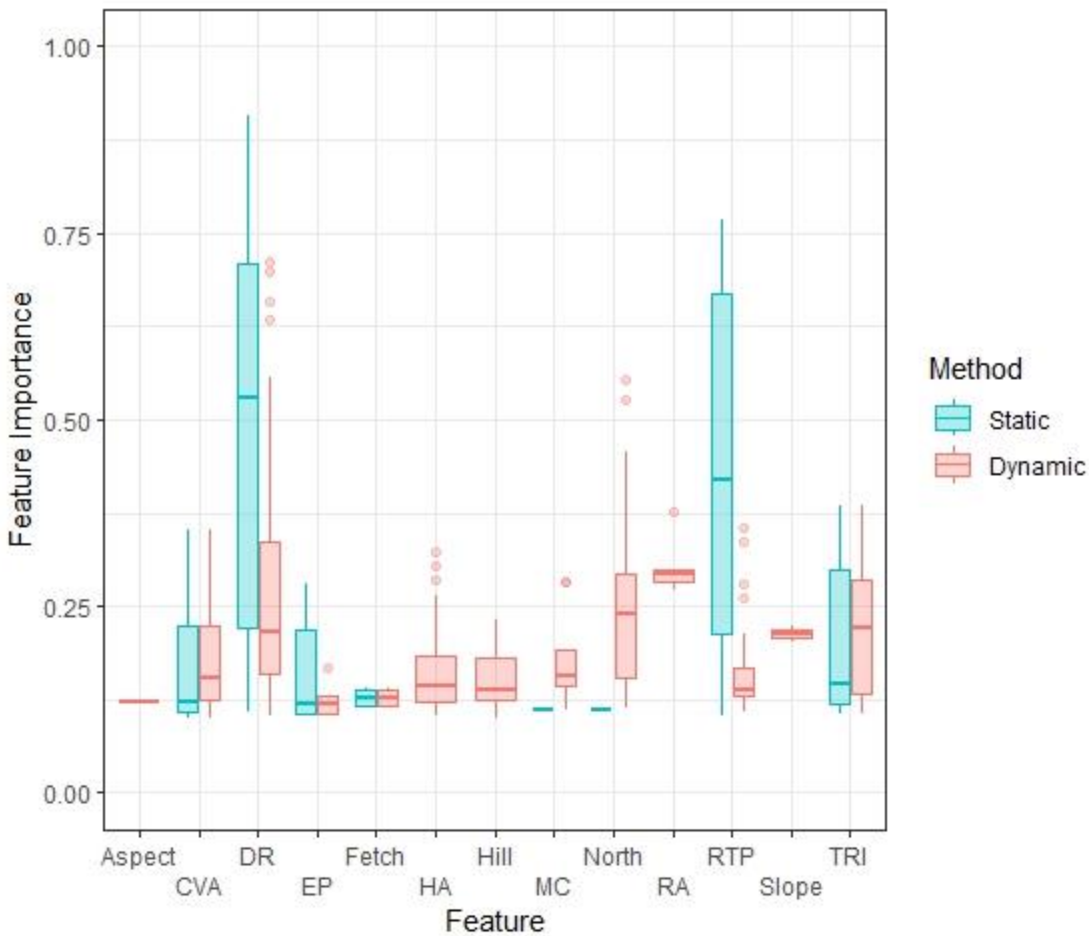

Figure 4-8. Topographic feature importance scores after removal of low importance scores (importance < 0.1). The static method had eight topographic features register importance scores above the threshold with Directional Relief (DR) and Relative Topographic Position (RTP) making the highest contributions to the snow depth estimates. The dynamic method had 13 topographic features with importance scores higher than the threshold.

4.2.3 Model Performance

Based on the Nash-Sutcliffe Efficiency (NSE), the dynamic model reached a maximum NSE of 0.97 (2/25/2020) and outperformed the static model by about 0.07 over most of the season with exception of the last observation (Figure 4-9a). The static method reached a maximum NSE of 0.92 on

2/11/2020. The maximum difference in NSE favoring the dynamic method was 0.09 (1/24/2020) and the maximum difference favoring the static method was 0.13 (3/24/2020). The average snow depth seen by each method was included to provide additional context for the two estimation models. The snow depth from the static method was larger than the dynamic method because the static method referenced the total snow accumulation whereas the dynamic method referenced the incremental snow accumulation or snow depth change from the perevious measurement date (Figure 4-9b).

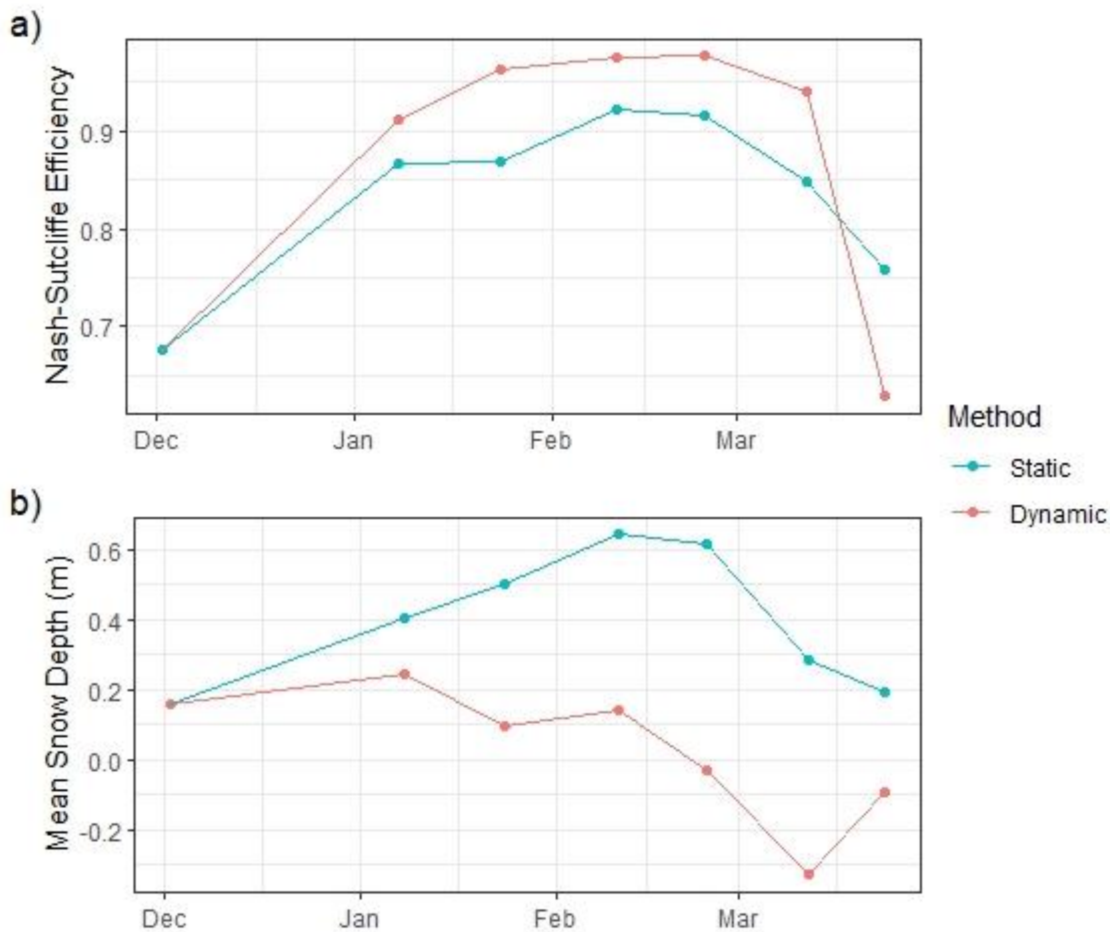

Figure 4-9. a) UPC average model NSE coefficients for static and dynamic methods. The dynamic method performed approximately 0.07 better than the static method excluding the last estimate. b) Average snow depth over the study period associated with each estimate method.

4.3 Izas Experimental Catchment Analysis

Snow depth at the Izas site was calculated from each TLS scan during the 2014 snow season using the static predecessor method (Figure 4-10). Snow depth patterns remain relatively consistent over the season with a majority of the catchment resulting in depths of 0-4 m. Small regions, predominantly in the south and north, consistently accumulated snow depths greater than 4 m. Holes within the catchment represent areas where the TLS instrument was obstructed from making depth measurements.

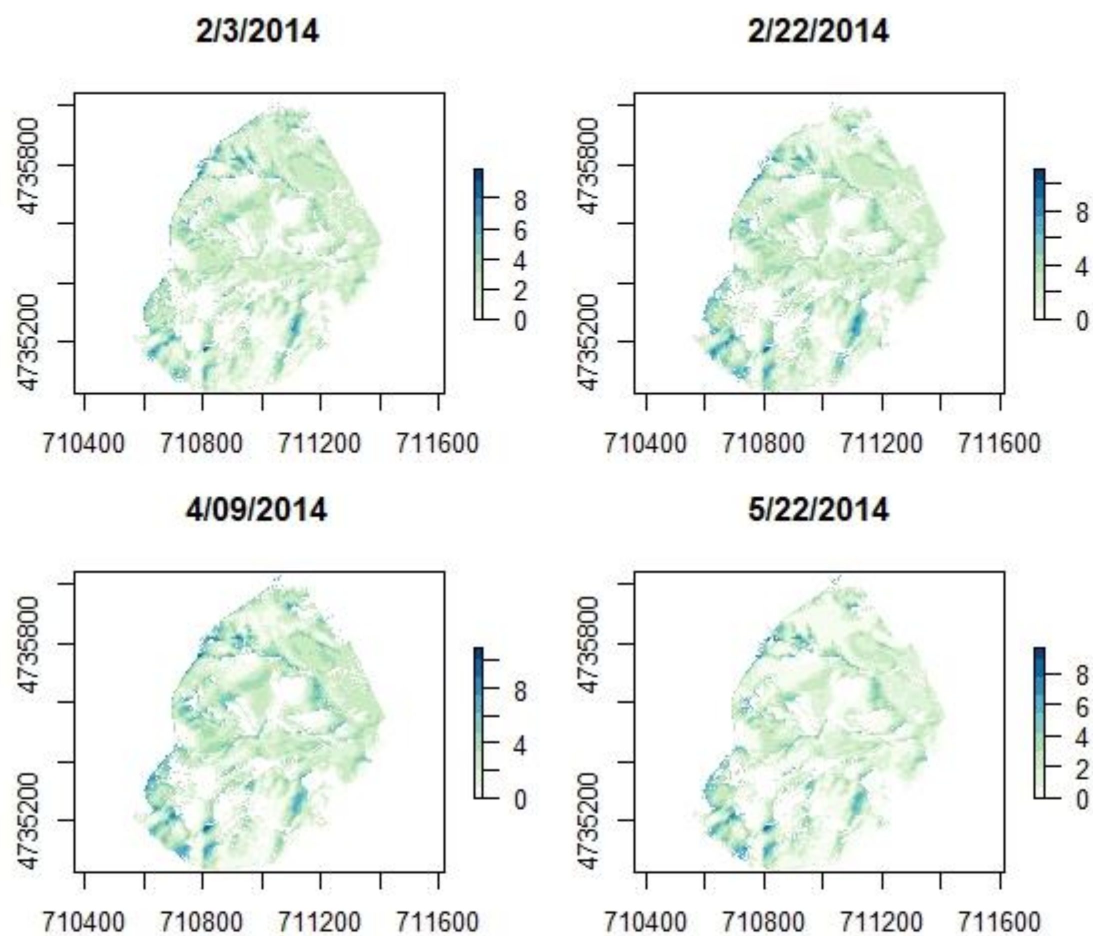

Figure 4-10. Snow accumulation patterns at Izas Experimental Catchment over the 2014 sampling period using the static surface differencing method and snow depth measured in meters. A majority of the catchment exhibits lower relative snow depths, while smaller localized areas consistently accumulate deep snow (dark blue areas).

From the static method, the features at the Izas catchment with the highest importance were Horizon Angle and Relative Topographic Position, with Directional Relief and Wind Fetch making minor contributions to snow depth estimates (Figure 4-11). The dynamic model had more features that provided meaningful contributions to the snow depth estimates to include: Aspect, Relative Aspect, Relative Topographic Position, Horizon Angle, Directional Relief, and Total Ruggedness Index. The topographic features from the dynamic model exhibited more temporal variability than those from the static model which in comparison remained relatively consistent over the observation period.

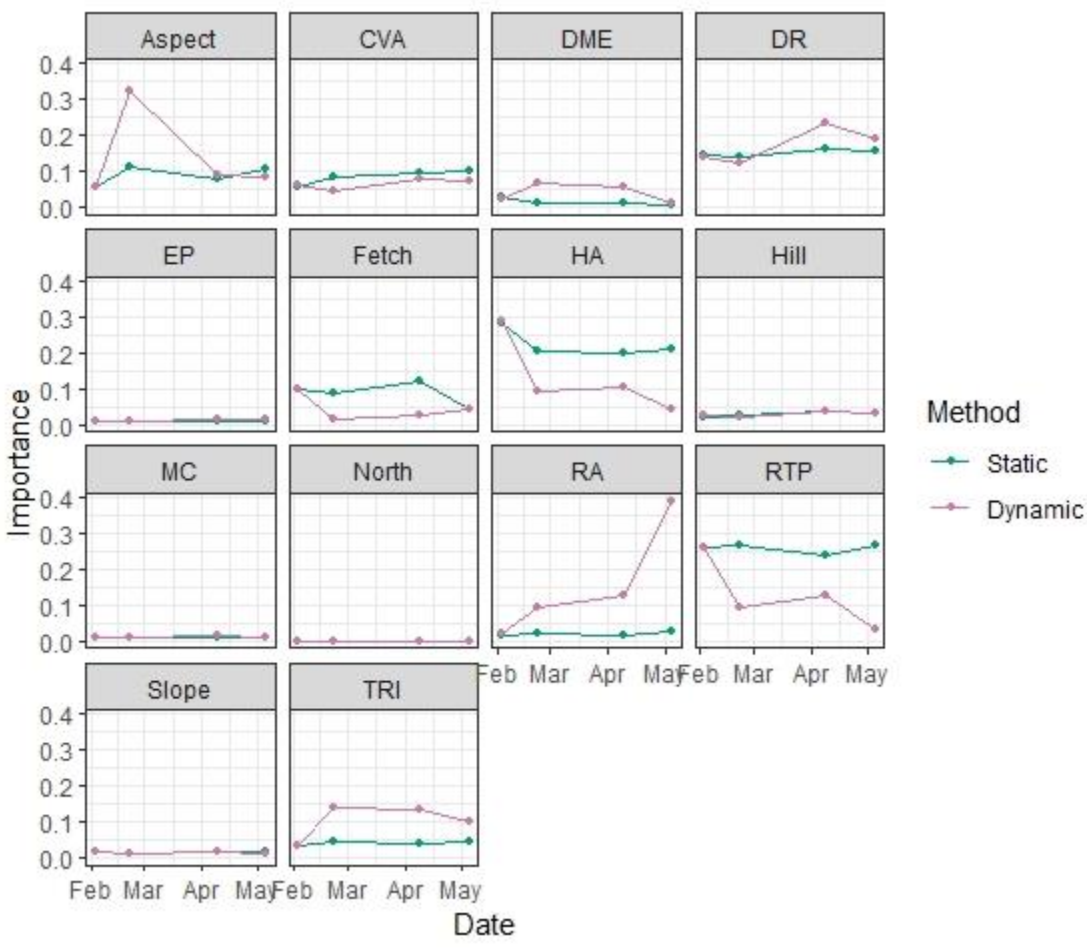

Figure 4-11. Individual feature importance time series for all topographic features computed for the static and dynamic snow estimation method at Izas. The static method feature importance is concentrated to Aspect, CVA, DR, Fetch, HA, and RTP. The dynamic method feature importance is made up of more topographic features including: Aspect, CVA, DR, DME, Fetch, HA, RA, RTP, and TRI.

From the static method, individual feature importance distribution minimum and maximum ranges and IQR's are small (Figure 4-12). Six topographic features registered importance over the threshold and Relative Topographic Position and Horizon Angle had the highest median importance. Distributions from the dynamic method exhibited more variability in individual feature importance than the static model. The minimum-maximum ranges and IQR's were both much greater than their static counterparts. A total of seven topographic features exceeded the threshold where Aspect and Relative Aspect displayed the highest median importance.

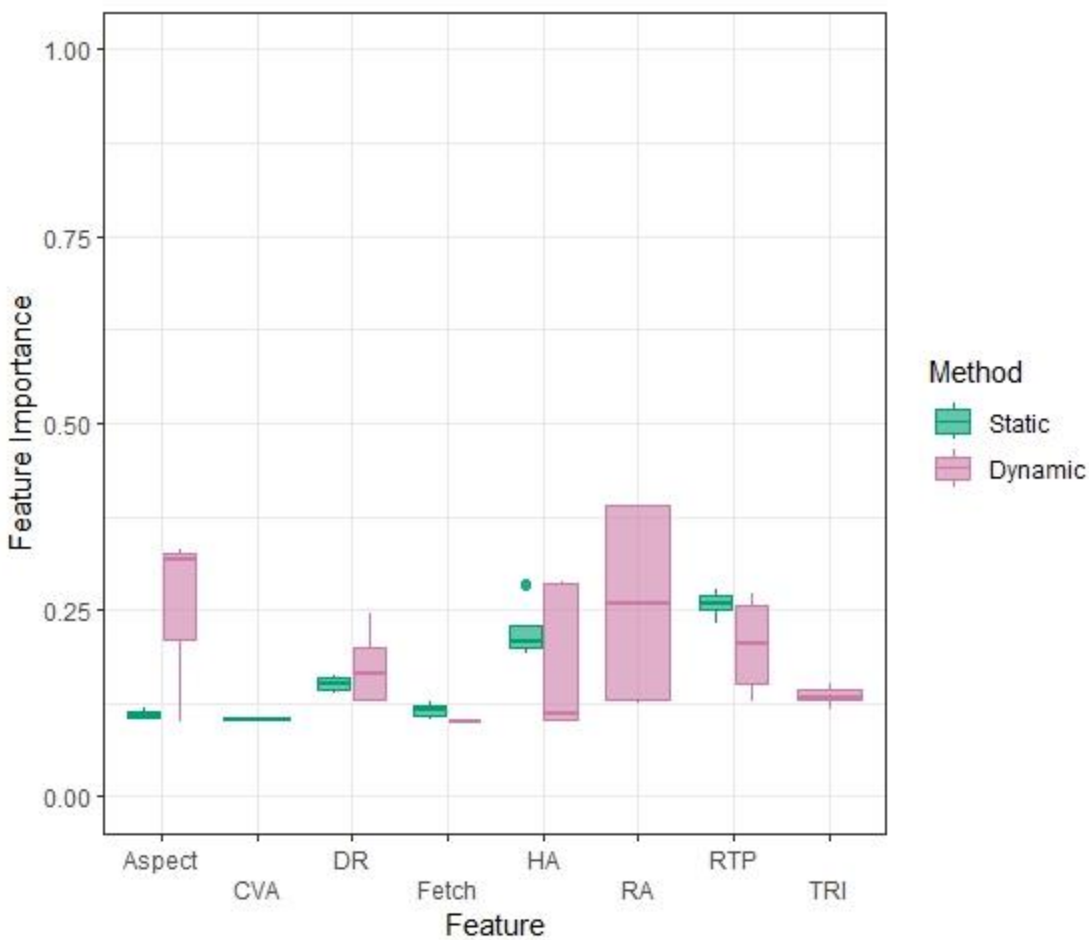

Figure 4-12. *Topographic feature importance scores after removal of low importance scores (importance < 0.1). The static method had six topographic features register importance scores above the threshold with Horizon Angle (HA) and Relative Topographic Position (RTP) making the highest contributions to the snow depth estimates. The*

dynamic method had 7 topographic features with importance scores higher than the threshold. The distributions from the dynamic method tended to be wider than those from the static method.

4.3.1 Izas Model Performance

In the Nash-Sutcliffe test between modeled and observed snow depth, three out of the four dynamic estimates performed better than the static method estimates (Figure 4-13a). The dynamic model outperformed the static model by approximately 0.01, whereas on the occasion where the reverse was true, the static model was approximately 0.05 better. As in the UPC experiment, the snow depth for the static model references total snow accumulation over the season, while the dynamic model represents the snow accumulated between samples (Figure 4-13b).

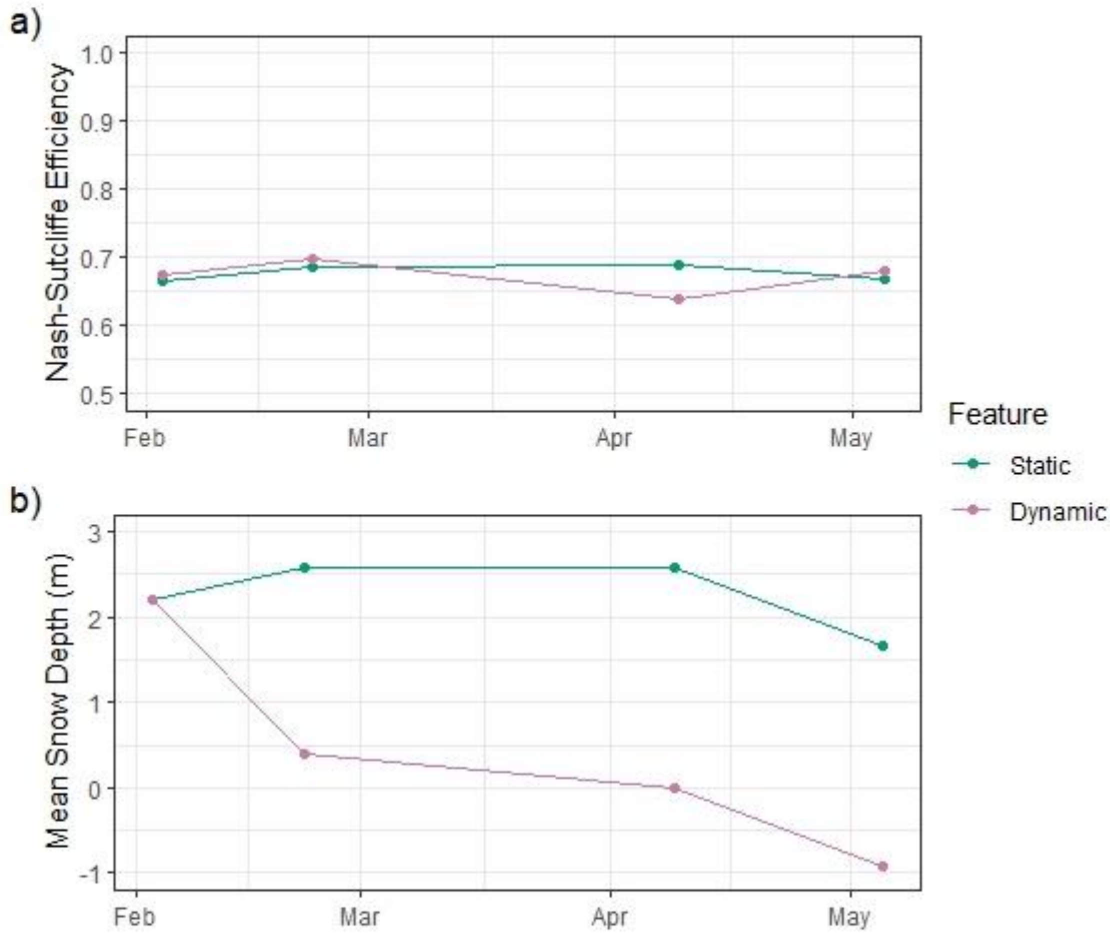

Figure 4-13. a) Izas average model NSE coefficients for static and dynamic methods. The dynamic model performed better by approximately 0.01 for three out of the four observations with the largest disparity occurring where the static model outperformed the dynamic method by approximately 0.05. b) Average snow depth over the study period associated with each method.

4.4 Site Comparison

The model performance was generally better at UPC than at Izas. At UPC using the 5 cm cropped extent, the NSE coefficients for both methods improved over the initial sampling period and fell towards the end (Figure 4-14a). At Izas, the NSE remained more constant over the duration of the observation period. The lowest average NSE coefficients from both methods at UPC are approximately even with the highest average NSE coefficients at Izas. When comparing the NSE distributions between snow depth estimation sites, Izas (n=16) displayed a narrower distribution and lower median than the NSE distributions from the UPC site (n=28) (Figure 4-14b). Considering the two depth estimation methods, the NSE distributions did not differ substantially between the static and dynamic models at Izas. However, at UPC, the distributions from the dynamic method had a wider IQR, larger total range, and higher median than the NSE from the static method.

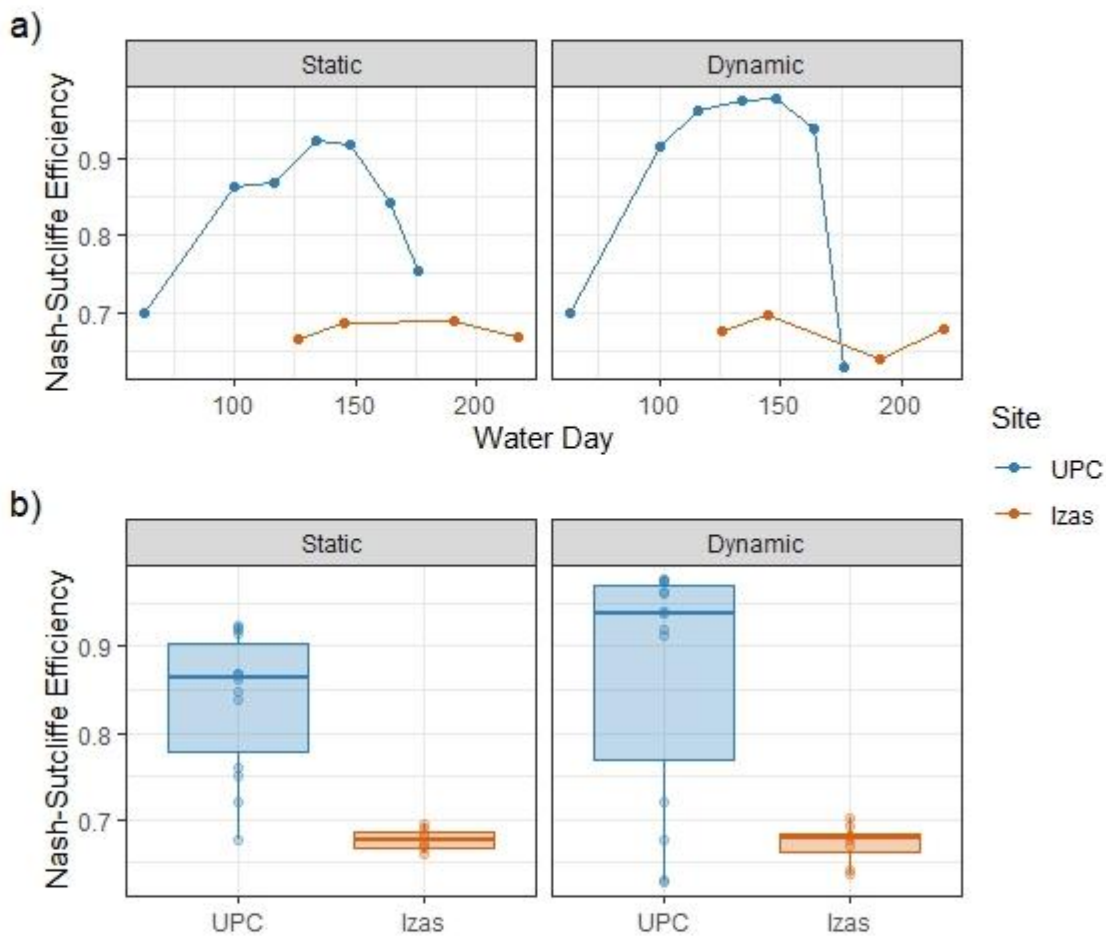

Figure 4-14. a) Mean NSE coefficients by site plotted on common water-day timeline displayed on the x-axis. The NSE coefficients from UPC are higher than the coefficients from Izas where the lowest coefficients from UPC are approximately even with the highest coefficients from Izas. b) Distribution of NSE scores by site and method. Between sites, Izas had lower average NSE and narrower distributions than UPC using the static and dynamic estimation methods.

5. DISCUSSION

Snow distribution modeling is a key area of research aimed at enhancing our understanding of the complex spatial and temporal distribution of snow. Traditionally, these models have relied on static representations of the snowfall affected surface, neglecting the dynamic nature of snow-affected topography and its influence on snow distribution. However, a novel approach has been implemented (Figure 3-1), incorporating dynamic topography as a key factor in snow accumulation modeling. This methodology recognizes the importance of accurately representing the evolving surface morphology and its impact on snow depth patterns. By considering dynamic topography, this modeling technique aims to provide a more representative depiction of the actual processes governing snow distribution.

Previous research has established the consistency of inter-seasonal spatial variability in snowpack, attributing it to the similarity of meteorological drivers, gradual land cover changes, and relatively stable topographical controls over time (Liston and Sturm, 1998; Deems et al., 2008; Sturm and Wagner, 2010; Mendoza et al., 2020). This study employs a unique approach by examining the intra-seasonal variability of snow distribution with a highly capable machine learning regression algorithm, a novel array of topographic features, and considers snow depth at spatial resolutions much finer than contemporary spatially distributed snow modeling, which typically range from meters to kilometers depending on the application objectives, computational resources, and level of detail required (Liston and Elder, 2006; Molotch and Margulis, 2008; Richter et al., 2021). To optimize a machine learning model, a common practice is hyper-parameter tuning, which involves systematically exploring different combinations of settings such as learning rate, regularization parameters, and depth. However, in our analysis, we decided not to undertake this time-consuming process due to the large number of models involved and previous research suggesting minimal impact on feature importance and model performance (Revuelto, 2020). By incorporating these alternative topographic variables at small spatial scales (Figure 4-1), the study expands our understanding of the complex interactions influencing snow distribution dynamics within a single snow season.

The sensitivity analysis conducted as part of the first objective yielded important insights into the behavior and characteristics of the static and dynamic machine learning based snow depth models. By varying parameters such as training data size and selection method, predominant wind direction used in feature creation, DEM resolution, scene extent, predictor feature length, and snowpack phase, we gained a deeper understanding of their effect on each model's behavior and performance over a single snow accumulation season. Through varying the size and selection style of model training data, a random selection method was more consistent among recommended partition sizes (70-80%) and resulted in lower evaluation metrics than training selection using a contiguous method (Figure 4-4). Next, the principal wind direction used for feature creation was changed to observe the effect on individual feature importance when estimating snow depth (Figure 4-5). Site specific wind direction was a critical factor for the creation and representation of wind-dependent topographic features used in model estimates and affected the relative importance metric of these features. The sensitivity analysis, which focused on the Directional Relief topographic feature, revealed that resolution had the most significant impact on the performance of both the static and dynamic snow accumulation models (Figure 4-5a). This sensitivity can be attributed to the different representations of spatial structures derived from the surface, which in turn affect the derived topographic features (Figure 3-5). The models exhibited a moderate sensitivity to the snowpack phase, where the dynamic model had higher Directional Relief importance during accumulation and the static model during net loss (Figure 4-5d). It is important to highlight that the primary focus of this methodology is on snow accumulation processes, and as such, the estimate of snow depth based on topographic surface features during ablation periods was not the intended application at the outset. Interestingly, changes in DEM extent and predictor variable lengths had minimal effects on topographic feature importance, indicating that these factors had a much lower influence on each model's behavior and overall performance (Figure 4-5b-c). These findings emphasize the value of selecting an appropriate DEM resolution and understanding the limitations of the models when applied to different snowpack phases.

The second objective of this study was to analyze the behavior of static and dynamic snow depth estimation models on a controlled dataset, focusing on their performance and characteristics throughout a single snow season. From the methodology (Figure 3-1) and results presented, we aimed to gain insights into their behaviors and reveal any distinct traits exhibited by each modeling approach. The analysis of the static and dynamic snow estimation models in the context of topographic feature importance time series analysis revealed distinct patterns in their behavior (Figure 4-2). Of the 14 snow depth predictors examined, the static model displayed a higher reliance on two key features, Directional Relief and Relative Topographic Position, and displayed a higher overall median feature importance over a single accumulation season (Figures 4-7 and 4-8). The estimates of snow depth were substantially influenced by these features, highlighting their strong association with accumulation processes. These findings align with previous studies that have utilized similar topographic features in various frameworks such as binary regression, multiple linear regression, and random forest machine learning (Revuelto et al., 2014; 2020). Differing from its role as a strong estimator of snow depth in earlier research (Molotch et al., 2005), Wind Fetch had a relatively milder influence on the estimates from the static model and was primarily associated with the initial accumulation of the snowpack. However, the low importance of Wind Fetch in this study may have been masked by the superior estimation capability of other wind related features such as Directional Relief, Horizon Angle, and Relative Aspect. In contrast to the static model, the dynamic model demonstrated a more diverse and nuanced approach, identifying a total of 13 different topographic features at a lower median importance value which were useful for snow depth estimates (Figures 4-2 and 4-8). This finding suggests that the dynamic model encompasses a broader set of factors and spatial structures to capture the intricate dynamics of snow accumulation tendencies. By incorporating a wider range of topographic features, the dynamic model allows for a better representation of the complex relationship between changing surface characteristics and snow distribution patterns within a single accumulation season.

The evaluation of the dynamic and static snow accumulation models based on the Nash-Sutcliffe snow depth performance metric revealed the superiority of the dynamic model over most of the sampling period (Figure 4-9). This improved performance can be attributed to the dynamic model's ability to leverage intra-seasonal structures of the snow-affected surface, resulting in a more accurate representation of actual snow accumulation processes. In contrast, the static model relied on a snow-free surface representation, which became anachronistic after ensuing snow depositions. The dynamic model's utilization of changing topography enabled it to adapt and account for the evolving snowpack surface, taking into consideration factors such as wind redistribution, snow-crystal metamorphism and settling, sublimation, and the changing spatial distribution of snowfall. Through the incorporation of these processes, the dynamic model demonstrated a higher degree of accuracy in snow depth estimates. In contrast, constrained by a fixed representation of the snow-free surface, the static model was unable to portray the evolving nature of the intra-seasonal snow surface and therefore exhibited lower performance.

The last objective of this study focused on evaluating the performance of machine learning snow accumulation methods under diverse conditions of location, scale, and sampling frequency. To assess the robustness and generalizability of these methods, a comparison was made between the models developed for the UPC site with models generated from Izas, which characterized an operationally representative hydrologic unit. To ensure the integrity of the modeling process, the models were individually developed at each site prior to comparison. This approach was necessary because tree-based models are highly sensitive to the training data they are provided, requiring comprehensive coverage of the full range of response values (Horning, 2010). As a result, the models lack transferability between different snow study sites, which aligns with the expected nature of these models (Erxleben et al., 2002; Revuelto et al., 2020). By examining the models' performance across different locations, scales, and temporal resolutions, valuable insights were gained regarding their ability to effectively capture and predict snow depth in distinct environments.

The comparison between the Izas Experimental Catchment and the UPC site was conducted by analyzing their NSE scores and distributions using the static and dynamic models. Notably, the dynamic method demonstrated greater improvement in performance at UPC compared to the Izas site (Figure 4-14a). Several factors could explain this disparity in model performance. The coarser resolution (1 m versus 5 cm) of the DEM at Izas likely impacted the representation of surface structures, resulting in different depictions of derived topographic features compared to UPC. At the Izas site, the extended interval between TLS scans permitted a greater opportunity for meteorological and environmental forcings to influence the snow-affected landscape. The lower frequency sampling increased the prevalence of unaccounted deposition events, wind redistribution, and sublimation which likely impacted the accuracy of the depth estimates and could explain the poor performance of the dynamic model, especially on the third sampling date (Figure 4-13a). Most notably, the two sites are situated in distinct locations and exhibit notable differences in scale. To assume the prevalence of similar meteorological conditions and process-scales at both sites would be erroneous (Blöschl, 1999), particularly given the alpine location of Izas and the potential intensity disparity of mechanisms like wind-scour and redistribution. Additionally, the increased terrain complexity at Izas resulted in a wider range of topographic feature values and an incomplete surface DEM which may have resulted in reduced performance (Figures 2-2c; 4-10). The holes in the DEM likely resulted from landform obstruction to TLS views despite using multiple acquisition locations. The unobserved regions could have a tendency for deeper accumulation zones and their exemption would introduce bias to the estimation models. Lastly, Izas (Figure 4-10) experienced approximately four times as much snow deposition as UPC (Figure 4-1), which may have posed challenges for the models to accurately estimate extreme snow depths (Revuelto et al., 2020). Taken together, these factors contribute to the observed differences in model performance between Izas and UPC, highlighting the importance of considering site-specific characteristics such as DEM and temporal resolution, terrain variability, and snow deposition magnitudes when evaluating the robustness and applicability of terrain-based machine learning snow accumulation models.

6. CONCLUSION

This study aimed to advance our understanding of snow accumulation mechanisms and the influence of scale on surface accumulation models while addressing the driving research questions, objectives, and hypothesis. The driving research questions involved the significance of intra-seasonal snowfall resurfacing on accumulation mechanisms and the impact of scale on variable surface accumulation models. The objectives were designed to conduct a sensitivity analysis to gain insights into the behavior of these models, explore the disparities between static and dynamic snow accumulation modeling approaches, and evaluate their performance under varying conditions. The proposed hypothesis that incorporating variable surface accumulation models that consider intra-seasonal snow resurfacing would produce more accurate snow depth estimates compared to accumulation models utilizing a static snow-free surface is supported through the methodology and results presented.

First, we performed a sensitivity analysis on the models to gain greater understanding of how they responded to changes in training data size and selection method, wind direction, resolution, extent, predictor size, and snowpack phase (Objective 1). We found that the models were susceptible to variations in training data size using a contiguous partition method, wind direction in feature creation, and input resolution where the patterns of the surface structure were represented differently according to cell resolution. As scale is coarsened the surface feature structures become subdued resulting in a decrease in importance from highly predictive features such as Directional Relief. The models demonstrated a notable level of resiliency when subjected to variations in training data sizes under the random selection method, DEM extents that may deviate from the actual ground surface representation, and the number of topographic features utilized for making depth estimates.

Next, using a constrained dataset at UPC, we compared the static and dynamic snow accumulation modeling approaches and revealed their differences in capturing the complexities of snow distribution (Objective 2). In the evaluation of topographic feature importance, we found that the dynamic model incorporated more surface features at lower median importance to use in the snow depth estimates over the course of a single accumulation season than the static surface model. In doing so, the dynamic surface model performed approximately 0.1 better than the static surface model in a Nash-Sutcliffe efficiency test. Through this analysis, we gained valuable insights into the characteristics and behavior of both static and dynamic models, shedding light on their strengths and limitations.

Finally, we evaluated the performance of machine learning snow accumulation methods under different conditions of location, scale, and temporal resolution by performing an analysis on a hydrologically operational dataset which aimed to assess the robustness and generalizability of the static and dynamic models (Objective 3). In moving to a site with much coarser cell-resolution, significantly larger area coverage, lower temporal resolution, and including more extreme terrain with an incomplete surface picture, we found that the models at Izas performed worse than those derived at UPC in a Nash-Sutcliffe efficiency analysis. In most cases at Izas where the dynamic model outperformed the static model, the average improvement was only approximately 0.01 on a Nash-Sutcliffe efficiency index. By subjecting the models to widely varying conditions, we examined their ability to adapt and provide reliable estimates of snow depth in diverse snow modeling regions and identify ways to improve their capability for further applications.

Through this research, we have advanced our understanding of snow accumulation mechanisms, the influence of scale on surface accumulation models, and the potential of dynamic models in improving snow depth estimations. We strongly recommend the integration of this approach to intra-seasonal snow accumulation modeling, which leverages the benefits of a variable surface, into the framework of relevant spatially distributed snow models such as iSnowbal (Marks et al., 1999), SnowModel (Liston and Elder, 2006), and Alpine3D (Lehning et al., 2006). While the machine learning algorithm employed in this study demonstrated site-specific effectiveness, the inclusion of more advanced artificial intelligence architectures, such as neural networks capable of spatiotemporal learning, would enhance snow accumulation modeling when applied in conjunction with a dynamic surface. The inclusion of airborne LiDAR acquisitions of the Izas site would further enhance this dataset for future use. A nadir perspective of the snow and ground surface would fill the topographic gaps created by obstructions to the TLS instrument and provide a more complete surface from which to model snow processes and reveal intra-seasonal behaviors. This knowledge is vital for enhancing water resource management, particularly in the context of climate change impacts, and provides a foundation for further advancements in snowpack modeling techniques.

REFERENCES

Alshari, H., Saleh, A.Y. and Odabaş, A., 2021. Comparison of gradient boosting decision tree algorithms for CPU performance. *Journal of Institue Of Science and Technology*, *37*(1), pp.157-168.

Alvera, B. and García-Ruiz, J.M., 2000. Variability of sediment yield from a high mountain catchment, Central Spanish Pyrenees. *Arctic, Antarctic, and Alpine Research*, *32*(4), pp.478-484.

Blöschl, G., 1999. Scaling issues in snow hydrology. *Hydrological processes*, *13*(14-15), pp.2149-2175.

Blue Maestro Tempo Disc™ Bluetooth Temperature & Humidity Sensor Beacon Logger. [Online] Available at: https://bluemaestro.com/products/tempo-disc-bluetooth-temperature-humidity-sensor-beacon-logger (Accessed: 13 October 2023).

Bormann, K.J., Westra, S., Evans, J.P. and McCabe, M.F., 2013. Spatial and temporal variability in seasonal snow density. *Journal of Hydrology*, *484*, pp.63-73.

Buisan, S.T., Saz, M.A. and López-Moreno, J.I., 2015. Spatial and temporal variability of winter snow and precipitation days in the western and central Spanish Pyrenees. *International Journal of Climatology*, *35*(2), pp.259-274.

Carroll, R.W., Deems, J.S., Niswonger, R., Schumer, R. and Williams, K.H., 2019. The importance of interflow to groundwater recharge in a snowmelt-dominated headwater basin. *Geophysical Research Letters*, *46*(11), pp.5899-5908.

Chen T., He T., Benesty M., Khotilovich V., Tang Y., Cho H., Chen K., Mitchell R., Cano I., Zhou T., Li M., Xie J., Lin M., Geng Y., Li Y., Yuan J., 2023. _xgboost: Extreme Gradient Boosting_. R package version 1.7.3.1, URL: (<https://CRAN.R-project.org/package=xgboost>).

Church, J.E., 1908. *The Mt. Rose Weather Observatory, 1906-1907: With Notes on the Progress of the Observatory, 1907-1908* (No. 67). University of Nevada.

Clark, M.P., Hendrikx, J., Slater, A.G., Kavetski, D., Anderson, B., Cullen, N.J., Kerr, T., Örn Hreinsson, E. and Woods, R.A., 2011. Representing spatial variability of snow water equivalent in hydrologic and land-surface models: A review. *Water Resources Research*, *47*(7).

CloudCompare (Version 2.10.2). [GPL software]. [Online] Available at: http://www.cloudcompare.org/.

Cohen, M., Christian-Smith, J. and Berggren, J., 2013. Water to supply the land. *Pac. Inst*.

Colbeck, S.C., 1982. An overview of seasonal snow metamorphism. *Reviews of Geophysics*, *20*(1), pp.45-61.

Deems, J.S., Fassnacht, S.R. and Elder, K.J., 2008. Interannual consistency in fractal snow depth patterns at two Colorado mountain sites. *Journal of Hydrometeorology*, *9*(5), pp.977-988.

Deems, J.S., Painter, T.H. and Finnegan, D.C., 2013. Lidar measurement of snow depth: a review. *Journal of Glaciology*, *59*(215), pp.467-479.

Doesken, N.J. and Judson, A., 1997. A guide to the science, climatology, and measurement of snow in the United States. *Colorado State University Department of Atmospheric Science, Fort Collins, CO*.

Döllner, J., 2020. Geospatial artificial intelligence: potentials of machine learning for 3D point clouds and geospatial digital twins. *PFG–Journal of Photogrammetry, Remote Sensing and Geoinformation Science*, *88*, pp.15-24.

Dozier, J., Bair, E.H. and Davis, R.E., 2016. Estimating the spatial distribution of snow water equivalent in the world's mountains. *Wiley Interdisciplinary Reviews: Water*, *3*(3), pp.461-474.

Egli, L., Jonas, T., Grünewald, T., Schirmer, M. and Burlando, P., 2012. Dynamics of snow ablation in a small Alpine catchment observed by repeated terrestrial laser scans. *Hydrological Processes*, *26*(10), pp.1574-1585.

Elder, K., Dozier, J. and Michaelsen, J., 1991. Snow accumulation and distribution in an alpine watershed. *Water Resources Research*, *27*(7), pp.1541-1552.

Erickson, T.A., Williams, M.W. and Winstral, A., 2005. Persistence of topographic controls on the spatial distribution of snow in rugged mountain terrain, Colorado, United States. *Water Resources Research*, *41*(4).

Erxleben, J., Elder, K. and Davis, R., 2002. Comparison of spatial interpolation methods for estimating snow distribution in the Colorado Rocky Mountains. *Hydrological Processes*, *16*(18), pp.3627-3649.

FARO Technologies, Inc. FARO Focus3D X 130 Laser Scanner: Technical Specification Sheet. [Online] Available at: https://knowledge.faro.com/Hardware/Focus/Focus (Accessed: 2 July 2023)

Fassnacht, S.R. and Deems, J.S., 2006. Measurement sampling and scaling for deep montane snow depth data. *Hydrological Processes: An International Journal*, *20*(4), pp.829-838.

Fassnacht, S.R., 2021. A call for more snow sampling. *Geosciences*, *11*(11), p.435.

Fassnacht, S.R., Brown, K.S.J., Blumberg, E.J., López Moreno, J.I., Covino, T.P., Kappas, M., Huang, Y., Leone, V. and Kashipazha, A.H., 2018. Distribution of snow depth variability. *Frontiers of Earth Science*, *12*, pp.683-692.

Glass, T.W., Breed, G.A., Liston, G.E., Reinking, A.K., Robards, M.D. and Kielland, K., 2021. Spatiotemporally variable snow properties drive habitat use of an Arctic mesopredator. *Oecologia*, *195*, pp.887-899.

Guan, B., Molotch, N.P., Waliser, D.E., Jepsen, S.M., Painter, T.H. and Dozier, J., 2013. Snow water equivalent in the Sierra Nevada: Blending snow sensor observations with snowmelt model simulations. *Water Resources Research*, *49*(8), pp.5029-5046.

Hagenstad, M.L., Burakowski, E.L. and Hill, R.L., 2018. The economics of snow for recreation in a changing climate. In *Proc. Int. Snow Science Workshop, Innsbruck, Austria, ISSW* (pp. 531-536).

Herbert, F., 1965. *Dune*. Chilton Books.

Hopkinson, C., Sitar, M., Chasmer, L. and Treitz, P., 2004. Mapping snowpack depth beneath forest canopies using airborne lidar. *Photogrammetric Engineering & Remote Sensing*, *70*(3), pp.323-330.

Horning, N., 2010. Random Forests: An algorithm for image classification and generation of continuous fields data sets.

Jonas, T., Marty, C. and Magnusson, J., 2009. Estimating the snow water equivalent from snow depth measurements in the Swiss Alps. *Journal of Hydrology*, *378*(1-2), pp.161-167.

Jordan, M.I. and Mitchell, T.M., 2015. Machine learning: Trends, perspectives, and prospects. *Science*, *349*(6245), pp.255-260.

Lange, H. and Sippel, S., 2020. Machine learning applications in hydrology. *Forest-water interactions*, pp.233-257.

Lefsky, M.A., Cohen, W.B., Parker, G.G. and Harding, D.J., 2002. Lidar remote sensing for ecosystem studies: Lidar, an emerging remote sensing technology that directly measures the three-dimensional distribution of plant canopies, can accurately estimate vegetation structural attributes and should be of particular interest to forest, landscape, and global ecologists. *BioScience*, *52*(1), pp.19-30.

Lehning, M., Völksch, I., Gustafsson, D., Nguyen, T.A., Stähli, M. and Zappa, M., 2006. ALPINE3D: a detailed model of mountain surface processes and its application to snow hydrology. *Hydrological Processes: An International Journal*, *20*(10), pp.2111-2128.

Lindsay, J.B., 2014, April. The whitebox geospatial analysis tools project and open-access GIS. In *Proceedings of the GIS Research UK 22nd Annual Conference, The University of Glasgow* (pp. 16-18).

Liston, G.E. and Elder, K., 2006. A distributed snow-evolution modeling system (SnowModel). *Journal of Hydrometeorology*, *7*(6), pp.1259-1276.

Liston, G.E. and Sturm, M., 1998. A snow-transport model for complex terrain. *Journal of Glaciology*, *44*(148), pp.498-516.

López-Moreno, J.I. and Nogués-Bravo, D., 2005. A generalized additive model for the spatial distribution of snowpack in the Spanish Pyrenees. *Hydrological Processes: An International Journal*, *19*(16), pp.3167-3176.

Lopez-Moreno, J.I. and Vicente-Serrano, S.M., 2007. Atmospheric circulation influence on the interannual variability of snow pack in the Spanish Pyrenees during the second half of the 20th century. *Hydrology Research*, *38*(1), pp.33-44.

López-Moreno, J.I., Fassnacht, S.R., Heath, J.T., Musselman, K.N., Revuelto, J., Latron, J., Morán-Tejeda, E. and Jonas, T., 2013. Small scale spatial variability of snow density and depth over complex alpine terrain: Implications for estimating snow water equivalent. *Advances in water resources*, *55*, pp.40-52.

Luce, C.H., Tarboton, D.G. and Cooley, K.R., 1998. The influence of the spatial distribution of snow on basin-averaged snowmelt. *Hydrological Processes*, *12*(10-11), pp.1671-1683.

Male, D.H. and Colbeck, S., 1980. The Seasonal Snow Cover. Dynamics of Snow and Ice Masses. *SC Colbeck*, pp.305-396.

Marks, D., Domingo, J., Susong, D., Link, T. and Garen, D., 1999. A spatially distributed energy balance snowmelt model for application in mountain basins. *Hydrological processes*, *13*(12-13), pp.1935-1959.

Mason, M.A., 2020. Snow Depth Distribution Patterns and Consistency from Airborne Lidar Time Series.

McCreight, J.L. and Small, E.E., 2013. Modeling bulk density and snow water equivalent using daily snow depth observations. *The Cryosphere Discussions*, *7*(5), pp.5007-5049.

Meiman, J.R., Froehlich, H.A. and Dils, R.E., 1969. *Snow accumulation in relation to forest canopy* (Doctoral dissertation, Colorado State University. Libraries).

Mendoza, P.A., Musselman, K.N., Revuelto, J., Deems, J.S., López-Moreno, J.I. and McPhee, J., 2020. Interannual and seasonal variability of snow depth scaling behavior in a subalpine catchment. *Water Resources Research*, *56*(7), p.e2020WR027343.

Mendoza, P.A., Shaw, T.E., McPhee, J., Musselman, K.N., Revuelto, J. and MacDonell, S., 2020. Spatial distribution and scaling properties of lidar-derived snow depth in the extratropical Andes. *Water Resources Research*, *56*(12), p.e2020WR028480.

Meromy, L., Molotch, N.P., Link, T.E., Fassnacht, S.R. and Rice, R., 2013. Subgrid variability of snow water equivalent at operational snow stations in the western USA. *Hydrological Processes*, *27*(17), pp.2383-2400.

Molotch, N.P. and Bales, R.C., 2005. Scaling snow observations from the point to the grid element: Implications for observation network design. *Water Resources Research*, *41*(11).

Molotch, N.P. and Margulis, S.A., 2008. Estimating the distribution of snow water equivalent using remotely sensed snow cover data and a spatially distributed snowmelt model: A multi-resolution, multi-sensor comparison. *Advances in water resources*, *31*(11), pp.1503-1514.

Moriasi, D.N., Arnold, J.G., Van Liew, M.W., Bingner, R.L., Harmel, R.D. and Veith, T.L., 2007. Model evaluation guidelines for systematic quantification of accuracy in watershed simulations. *Transactions of the ASABE*, *50*(3), pp.885-900.

Myers, T., 2013. Loss rates from Lake Powell and their impact on management of the Colorado River. *JAWRA Journal of the American Water Resources Association*, *49*(5), pp.1213-1224.

Nash, J.E. and Sutcliffe, J.V., 1970. River flow forecasting through conceptual models part I—A discussion of principles. *Journal of hydrology*, *10*(3), pp.282-290.

Oroza, C.A., Zheng, Z., Glaser, S.D., Tuia, D. and Bales, R.C., 2016. Optimizing embedded sensor network design for catchment-scale snow-depth estimation using LiDAR and machine learning. *Water Resources Research*, *52*(10), pp.8174-8189.

Painter, T.H., Berisford, D.F., Boardman, J.W., Bormann, K.J., Deems, J.S., Gehrke, F., Hedrick, A., Joyce, M., Laidlaw, R., Marks, D. and Mattmann, C., 2016. The Airborne Snow Observatory: Fusion of scanning lidar, imaging spectrometer, and physically-based modeling for mapping snow water equivalent and snow albedo. *Remote Sensing of Environment*, *184*, pp.139-152.

Peixóto, J.P. and Oort, A.H., 1984. Physics of climate. *Reviews of Modern Physics*, *56*(3), p.365.

Pomeroy, J. W., Parviainen, J., Hedstrom, N., & Gray, D. M. (1998). Coupled modelling of forest snow interception and sublimation. *Hydrological processes*, *12*(15), 2317-2337.

Pomeroy, J., MacDonald, M., DeBeer, C. and Brown, T., 2009, April. Modelling alpine snow hydrology in the Canadian Rocky Mountains. In *Western Snow Conference 2009*.

QGIS.org 2022, 'QGIS Geographic Information System (Version 3.16.7)', QGIS Association. Available at: http://www.qgis.org.

R Core Team 2023, R: A language and environment for statistical computing, R Foundation for Statistical Computing, Vienna, Austria. Available at: https://www.R-project.org.

Revuelto, J., Azorin-Molina, C., Alonso-González, E., Sanmiguel-Vallelado, A., Navarro-Serrano, F., Rico, I. and López-Moreno, J.I., 2017. Meteorological and snow distribution data in the Izas Experimental Catchment (Spanish Pyrenees) from 2011 to 2017. *Earth System Science Data*, *9*(2), pp.993-1005.

Revuelto, J., Billecocq, P., Tuzet, F., Cluzet, B., Lamare, M., Larue, F. and Dumont, M., 2020. Random forests as a tool to understand the snow depth distribution and its evolution in mountain areas. *Hydrological Processes*, *34*(26), pp.5384-5401.

Revuelto, J., López-Moreno, J.I., Azorín-Molina, C., Zabalza, J., Arguedas, G. and Vicente-Serrano, S.M., 2014. Mapping the annual evolution of snow depth in a small catchment in the Pyrenees using the long-range terrestrial laser scanning. *Journal of Maps*, *10*(3), pp.379-393.

Richter, B., Schweizer, J., Rotach, M.W. and van Herwijnen, A., 2021. Modeling spatially distributed snow instability at a regional scale using Alpine3D. *Journal of Glaciology*, *67*(266), pp.1147-1162.

Schaefli, B., Hingray, B. and Musy, A., 2007. Climate change and hydropower production in the Swiss Alps: quantification of potential impacts and related modelling uncertainties. *Hydrology and Earth System Sciences*, *11*(3), pp.1191-1205.

Schmidt, R.A., 1982. Properties of blowing snow. *Reviews of Geophysics*, *20*(1), pp.39-44.

Serreze, M.C., Clark, M.P., Armstrong, R.L., McGinnis, D.A. and Pulwarty, R.S., 1999. Characteristics of the western United States snowpack from snowpack telemetry (SNOTEL) data. *Water Resources Research*, *35*(7), pp.2145-2160.

Sturm, M. and Wagner, A.M., 2010. Using repeated patterns in snow distribution modeling: An Arctic example. *Water Resources Research*, *46*(12).

Sturm, M., Goldstein, M.A. and Parr, C., 2017. Water and life from snow: A trillion dollar science question. *Water Resources Research*, *53*(5), pp.3534-3544.

U.S. Bureau of Reclamation 2012, 'Colorado River Basin Water Supply and Demand Study', [Online] Available at: http://www.usbr.gov/lc/region/programs/crbstudy.html (Accessed: 13 October 2023).

U.S. Geological Survey 2022, 'Water Science School: The Water Cycle', [Online] Available at: https://www.usgs.gov/special-topics/water-science-school/science/water-cycle (Accessed: 13 October 2023).

U.S. Department of Agriculture, Natural Resources Conservation Service, 'NRCS SNOTEL (Snow Telemetry) System'. Available at: https://www.wcc.nrcs.usda.gov/snow/ (Accessed: 13 October 2023).

Winstral, A. and Marks, D., 2002. Simulating wind fields and snow redistribution using terrain-based parameters to model snow accumulation and melt over a semi-arid mountain catchment. *Hydrological Processes*, *16*(18), pp.3585-3603.

Zhang, W., Qi, J., Wan, P., Wang, H., Xie, D., Wang, X. and Yan, G., 2016. An easy-to-use airborne LiDAR data filtering method based on cloth simulation. *Remote sensing*, *8*(6), p.501.